PHYSICAL REVIEW D **87,** 074501 (2013)

Lattice QCD study of the s-wave $\pi\pi$ scattering lengths in the $I = 0$ and 2 channels

Ziwen Fu*

Key Laboratory for Radiation Physics and Technology of Education Ministry; Institute of Nuclear Science and Technology, College of Physical Science and Technology, Sichuan University, Chengdu 610064, People's Republic of China

(Received 28 January 2013; revised manuscript received 4 March 2013; published 2 April 2013)

The s-wave pion-pion ($\pi\pi$) scattering lengths are computed below the inelastic threshold by the Lüscher technique with pion masses ranging from 240 to 463 MeV. In the Asqtad-improved staggered fermion formulation, we calculate the $\pi\pi$ four-point functions for the $I = 0$ and 2 channels with "moving" wall sources without gauge fixing, and we analyze them at the next-to-leading order in the continuum three-flavor chiral perturbation theory. At the physical pion mass, we secure the s-wave $\pi\pi$ scattering lengths as $m_\pi a_{\pi\pi}^{I=0} = 0.214(4)(7)$ and $m_\pi a_{\pi\pi}^{I=2} = -0.04430(25)(40)$ for the $I = 0$ and 2 channels, respectively, where the first uncertainties are statistical and the second ones are our estimates of several systematic effects. Our lattice results for the s-wave $\pi\pi$ scattering lengths are in good accordance with available experimental reports and theoretical forecasts at low momentum. A basic ingredient in our study for the $I = 0$ case is properly incorporating the disconnected diagram. These lattice computations are carried out with the MILC $2 + 1$ flavor gauge configurations at two lattice spacings, $a \approx 0.15$ and 0.12 fm.

DOI: 10.1103/PhysRevD.87.074501 PACS numbers: 12.38.Gc, 11.15.Ha

I. INTRODUCTION

The research on $\pi\pi$ scattering is a basic and classical subject in the field of strong hadronic interactions. Its manageability and simplicity essentially stem from the pseudo-Nambu-Goldstone boson nature of the pion, a natural aftermath of the spontaneous chiral symmetry breaking in quantum chromodynamics (QCD), which imposes rigid constraints on $\pi\pi$ low-energy interactions. Moreover, the s-wave $\pi\pi$ scattering lengths vanish in the chiral limit when the momentum of the pions approaches zero. Since these quantities stand for a sensitive probe of the chiral symmetry breaking generated by the quark masses, the lattice QCD study, an objective of this paper, is a nonperturbative method we use in an effort to comprehend the low-energy nature of QCD.

With small pion masses and low momenta, the s-wave $\pi\pi$ scattering lengths can be solely predicted at leading order (LO) in chiral perturbation theory (χPT) [1]. The next-to-leading order (NLO) and next-to-next-to-leading order (NNLO) corrections in the chiral expansion [2–4] lead to perturbative deviations from the LO and involve both computable nonanalytic contributions and analytic terms with some unknown low-energy constants (LECs), which can be obtained from lattice simulations or experimental measurements.

A combination of some experimental and theoretical inputs from Colangelo *et al.* [3,4], along with the Roy equation [5,6], produced a precise result of the s-wave $\pi\pi$ scattering lengths. Zhou *et al.* studied the pole structure of the low-energy $\pi\pi$ scattering amplitudes using a proper chiral unitarization method in addition to the crossing symmetry and low-energy phase shift data, and they estimated the s-wave $\pi\pi$ scattering lengths [7]. K. Sasaki and N. Ishizuka found that the scattering phase can be obtained directly from the $\pi\pi$ wave function [8]. Guo *et al.* provided a reliable and solid estimation of all parts of the $\mathcal{O}(p^6)$ calculation [9], and some resonance contributions were added in to the former phenomenological calculations [3,4]. They also obtained slight differences with respect to previous results in Refs. [3,4]. Using the NLO $SU(2)$ unitary chiral perturbation theory to examine $\pi\pi$ scattering, Albaladejo and Oller obtained a good reproduction of the s-wave $\pi\pi$ scattering lengths [10].

In conjunction with the strict χPT constraints in the analysis, a considerably improved accuracy for the s-wave $\pi\pi$ scattering lengths has been obtained from the experimental measurement of the semileptonic K_{e4} decay by E865 [11]. With the independent experimental uncertainties and different theoretical inputs [3,4,12], the NA48/2 high-precision analyses of the K_{e4} and $K_{3\pi}$ decays [13–16] gave rise to the complementary information on the s-wave $\pi\pi$ scattering lengths [15]. All of these theoretical (or phenomenological) predictions and experimental determinations are consistent with one another.

Lattice studies of $\pi\pi$ scattering have been conducted in quenched QCD by various groups [17–23]. The full lattice study of the s-wave $I = 2$ $\pi\pi$ scattering length was first carried out by CP-PACS [24]. Fully dynamical computation of $I = 2$ $\pi\pi$ scattering was explored by NPLQCD with the domain-wall valence quarks on fourth-rooted staggered sea quarks [25,26]. Using the $N_f = 2$ maximally twisted mass fermion ensembles, Xu *et al.* employed the lightest pion mass at that time and conducted an explicit check for lattice artifacts [27]. With an anisotropic $N_f = 2 + 1$ clover fermion discretization, the $I = 2$ $\pi\pi$

*fuziwen@scu.edu.cn

scattering phase shift is calculated by NPLQCD to determine all of the threshold parameters [28]. Moreover, efforts were made to first secure the d-wave $I = 2$ $\pi\pi$ phase shift in some nice works by HSC [29,30]. Using overlap fermion formulation, Yagi *et al.* examined the consistency of the lattice data with the NNLO χPT prediction after correcting finite volume effects [31].

Nevertheless, only a couple of lattice studies in the $I=0$ channel have been reported so far whose computations are hindered by the so-called "disconnected diagram." Using the quenched approximation, Kuramashi *et al.* carried out the pioneering work for isospin-0; however, the vacuum diagram was disregarded, assuming that vacuum amplitude remains small for large t [18]. Additionally, for the rectangular and vacuum diagrams, quark loops are required to make the scattering amplitudes unitary; otherwise, the basic part of the physics is lost due to quenched approximation [17]. Liu conducted the first full QCD calculation for the $I = 0$ channel including the vacuum graph; however, the error of the extracted scattering length is remarkably large due to the usage of big pion masses (a small one is 430 MeV) [32]. With the presence of the vacuum diagram, we have attempted to crudely calculate $\pi\pi$ scattering for isospin-0, and we have made a first lattice calculation for $l_{\pi\pi}^{I=0}(\mu)$, which is a LEC appearing in the χPT expression of the $\pi\pi$ scattering length for isospin-0 [33]. Nonetheless, we used the partially quenched QCD to save computational cost, and worked with large quark masses [33]. Moreover, the statistical errors are underestimated, since we only considered the primary one [33]. Furthermore, we neglected the obvious oscillating term due to the staggered scheme. We understood that the statistical errors for the ratio of vacuum amplitudes grow as $e^{2m_\pi t}$ [34]. Consequently, using the small quark mass is very important for the $I = 0$ channel. As presented later, our lattice results will indeed quantitatively confirm this argument, and we acquire good signals of the vacuum diagram for the lattice ensembles with small pion masses.

To overcome the Maiani-Testa theorem [35], researchers usually calculate the energy levels of a two- (many-) particle system enclosed in a torus, so that its scattering amplitudes can be recovered [36–49]. In this work, Lüscher's technique [36–38] is employed to extract the scattering phase shift with the lattice-calculated energy eigenstates.

We here use the MILC gauge configurations [50,51] with the $2 + 1$ flavors of the Asqtad-improved staggered dynamical quarks [52] to compute the s-wave $\pi\pi$ scattering lengths. The technique of the "moving" wall source without gauge fixing [53], first introduced in Refs. [18,19], is exploited to calculate all four diagrams classified in Refs. [17–19], and special effort is payed to the disconnected diagram. Our lightest pion mass is about 240 MeV, which is lighter than those of the former lattice studies on $\pi\pi$ scattering and enables us to further explore the chiral limit. Consequently, the signals of the vacuum diagram are remarkably improved. Moreover, due to the nature of staggered fermions, our computations are automatically precise to $\mathcal{O}(a^2)$ [17]. Additionally, we used the continuum three-flavor χPT at NLO to extrapolate our lattice-measured $\pi\pi$ scattering lengths to the physical point. As presented later, we find

$$m_\pi a_{\pi\pi}^{I=2} = -0.04430(25)(40);$$
$$l_{\pi\pi}^{I=2} = 3.27(.77)(1.12),$$

where $a_{\pi\pi}^{I=2}$ denote the s-wave $\pi\pi$ scattering lengths in the $I = 2$ channel and $l_{\pi\pi}^{I=2}(\mu)$ is a LEC evaluated at the physical pion decay constant. These results are in good agreement with experimental measurements and theoretical (or phenomenological) determinations, as well as previous lattice calculations. Mostly, we obtain

$$m_\pi a_{\pi\pi}^{I=0} = 0.214(4)(7); \qquad l_{\pi\pi}^{I=0} = 43.2(3.5)(5.6),$$

which are in fair accordance with experimental reports and theoretical (or phenomenological) predictions, and which significantly improve our former study in Ref. [33].

The paper is organized as follows. In Sec. II we will review the basic formalism for the calculation of s-wave $\pi\pi$ scattering [37,38]. The simulation parameters and our concrete lattice calculations are shown in Sec. III. We will give the results of the lattice simulation data in Sec. IV, fitting analyses in Sec. V, and chiral extrapolation along with the comparisons of different results in Sec. VI. Finally, a summary of the conclusions and outlooks we arrived at are given in Sec. VII. The compact continuum three-flavor χPT forms at NNLO for the $\pi\pi$ scattering lengths are courteously dedicated to the Appendix.

II. METHOD

On the basis of the original derivations and notations in Refs. [17–19], we reviewed the indispensable formulas for the lattice QCD evaluation of the s-wave $\pi\pi$ scattering lengths in a torus. The formulas and the notations adopted here are actually the same as those in Refs. [33,54]. But, to make this paper self-supporting, all the essential parts will be reiterated subsequently.

Let us review scattering of two Nambu-Goldstone pions in the Asqtad-improved staggered fermion formalism. For s-wave $\pi\pi$ scattering, only the isospin $I = 0$ and 2 channels are permitted, owing to Bose symmetry. We build these $\pi\pi$ isospin eigenchannels using the following interpolating operators [18,19]:

$$\mathcal{O}_{\pi\pi}^{I=0}(t) = \frac{1}{\sqrt{3}}\{\pi^-(t)\pi^+(t+1) + \pi^+(t)\pi^-(t+1) - \pi^0(t)\pi^0(t+1)\},$$
$$\mathcal{O}_{\pi\pi}^{I=2}(t) = \pi^+(t)\pi^+(t+1), \tag{1}$$

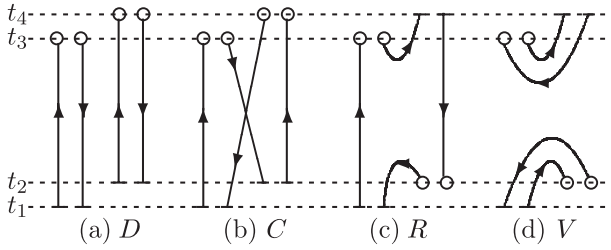

FIG. 1. Quark-line diagrams contributing to $\pi\pi$ four-point functions. Short bars indicate the wall sources. The wall sinks for local pion operators are represented by open circles.

with the interpolating pion operators denoted by

$$\pi^+(t) = -\sum_{\mathbf{x}} \bar{d}(\mathbf{x}, t)\gamma_5 u(\mathbf{x}, t),$$
$$\pi^-(t) = \sum_{\mathbf{x}} \bar{u}(\mathbf{x}, t)\gamma_5 d(\mathbf{x}, t),$$
$$\pi^0(t) = \frac{1}{\sqrt{2}}\sum_{\mathbf{x}}[\bar{u}(\mathbf{x}, t)\gamma_5 u(\mathbf{x}, t) - \bar{d}(\mathbf{x}, t)\gamma_5 d(\mathbf{x}, t)].$$

Then we express the $\pi\pi$ four-point function in the zero momentum state as

$$C_{\pi\pi}(t_1, t_2, t_3, t_4) = \sum_{\mathbf{x}_1}\sum_{\mathbf{x}_2}\sum_{\mathbf{x}_3}\sum_{\mathbf{x}_4}\langle \mathcal{O}_\pi(\mathbf{x}_4, t_4)\mathcal{O}_\pi(\mathbf{x}_3, t_3) \times \mathcal{O}^\dagger_\pi(\mathbf{x}_2, t_2)\mathcal{O}^\dagger_\pi(\mathbf{x}_1, t_1)\rangle,$$

where, to prevent the intricate color Fierz rearrangement of the quark lines [18,19],[1] we familiarly select $t_1 = 0$, $t_2 = 1$, $t_3 = t$, and $t_4 = t + 1$ [18,19].

In the isospin limit, only four diagrams contribute to $\pi\pi$ scattering amplitudes; in Fig. 1, we show these quark-line diagrams, which are identified as direct (D), crossed (C), rectangular (R), and vacuum (V) diagrams, respectively [18,19]. A reliable evaluation of the rectangular diagram is challenging and a rigorous computation of the vacuum diagram is fairly difficult [18,19].

In our former works [33,54], we calculated these four diagrams via evaluating T quark propagators [18,19]:

$$\sum_x D_{n,x}G_t(x) = \sum_{\mathbf{x}}\delta_{n,(\mathbf{x},t)}, \qquad 0 \le t \le T-1.$$

The combination of $G_t(n)$ which we apply for the $\pi\pi$ four-point functions is schematically illustrated in Fig. 1, and these diagrams can be described by means of G:

$$C^D(t_1, t_2, t_3, t_4) = \sum_{\mathbf{x}_3}\sum_{\mathbf{x}_4}\langle \mathrm{Tr}[G^\dagger_{t_1}(\mathbf{x}_3, t_3)G_{t_1}(\mathbf{x}_3, t_3)]\,\mathrm{Tr}[G^\dagger_{t_2}(\mathbf{x}_4, t_4)G_{t_2}(\mathbf{x}_4, t_4)]\rangle,$$
$$C^C(t_1, t_2, t_3, t_4) = \sum_{\mathbf{x}_3}\sum_{\mathbf{x}_4}\langle \mathrm{Tr}[G^\dagger_{t_1}(\mathbf{x}_3, t_3)G_{t_2}(\mathbf{x}_3, t_3)G^\dagger_{t_2}(\mathbf{x}_4, t_4)G_{t_1}(\mathbf{x}_4, t_4)]\rangle,$$
$$C^R(t_1, t_2, t_3, t_4) = \sum_{\mathbf{x}_2,\mathbf{x}_3}\langle \mathrm{Tr}[G^\dagger_{t_1}(\mathbf{x}_2, t_2)G_{t_4}(\mathbf{x}_2, t_2)G^\dagger_{t_4}(\mathbf{x}_3, t_3)G_{t_1}(\mathbf{x}_3, t_3)]\rangle,$$
$$C^V(t_1, t_2, t_3, t_4) = \sum_{\mathbf{x}_2}\sum_{\mathbf{x}_3}\{\langle \mathrm{Tr}[G^\dagger_{t_1}(\mathbf{x}_2, t_2)G_{t_1}(\mathbf{x}_2, t_2)]\,\mathrm{Tr}[G^\dagger_{t_4}(\mathbf{x}_3, t_3)G_{t_4}(\mathbf{x}_3, t_3)]\rangle - \langle \mathrm{Tr}[G^\dagger_{t_1}(\mathbf{x}_2, t_2)G_{t_1}(\mathbf{x}_2, t_2)]\rangle\langle \mathrm{Tr}[G^\dagger_{t_4}(\mathbf{x}_3, t_3)G_{t_4}(\mathbf{x}_3, t_3)]\rangle\}, \quad (2)$$

where the indicated traces are conducted over color, the γ^5 factors are neatly removed using the Hermiticity attributes of the propagator G, and a vacuum deduction is a natural companion to the vacuum diagram [56].

The rectangular and vacuum diagrams inevitably create the gauge-variant noise [18,19], which is neatly diminished by executing the gauge field average without gauge fixing, as we practiced in Refs. [33,53,54,57–60]. In the isospin limit, the $\pi\pi$ four-point functions for the $I = 0$ and 2 channels can be expressed on the strength of four diagrams [17–19]:

$$C^{I=0}_{\pi\pi}(t) \equiv \langle \mathcal{O}^{I=0}_{\pi\pi}(t)|\mathcal{O}^{I=0}_{\pi\pi}(0)\rangle = D + \frac{N_f}{2}C - 3N_f R + \frac{3}{2}V,$$
$$C^{I=2}_{\pi\pi}(t) \equiv \langle \mathcal{O}^{I=2}_{\pi\pi}(t)|\mathcal{O}^{I=2}_{\pi\pi}(0)\rangle = D - N_f C, \quad (3)$$

where the staggered-flavor factor N_f is inserted to rectify for the extra factor N_f in the valence fermion loops [17]. The fourfold degeneracy of the staggered sea quarks is removed by conducting the quadruple root of the fermion determinant [17,61]. The fourth-root recipes are assumed to be able to restore the right continuum limit of QCD [61], and our results rest on this hypothesis. See Ref. [62] for more discussions about the fourth-root trick.

It is customary to make use of the effective range expansion for parametrizing the low-momentum behavior of the s-wave $\pi\pi$ scattering phase δ_0,

$$k\cot\delta_0(k) = \frac{1}{a} + \frac{1}{2}rk^2 + \mathcal{O}(k^4), \quad (4)$$

[1]Fierz contributions force us to overcome the obstacle due to the staggered-flavor symmetry breaking [17]. The same problem is also encountered for πK scattering, which is addressed by Lang *et al.* in Ref. [55]. In principle, they can be disentangled by the method discussed in Ref. [17], but this is strenuous in practice. Fortunately, it can be trivially handled by the method introduced in Refs. [18,19]; i.e., π meson operators are separated by a unit time slice.

TABLE I. The parameters of MILC gauge configurations used in the present work. The lattice dimensions are expressed in lattice units in the second column with spatial (L) and temporal (T) size. The gauge coupling $\beta = 10/g^2$ is shown in column 3. The fourth and fifth columns give the bare masses of the light and strange quark masses in terms of am_l and am_s, respectively. The tadpole-improvement factor u_0 is listed in column 6. The ratio r_1/a is provided in column 7 (see Ref. [74] for the MILC definition of r_1). The inverse lattice spacing a^{-1} is recapitulated in column 8 [for the (0.00484, 0.0484) ensemble, we obtain the value of r_1/a from Ref. [70] and then calculate a^{-1}]. In the last column, the numbers of gauge configurations are given.

Ensemble	$L \times T$	β	am_l	am_s	u_0	r_1/a	a^{-1} GeV	N_{cf}
			$a \approx 0.12$ fm					
2464f21b676m005m050	$24^3 \times 64$	6.76	0.005	0.050	0.8678	2.647(3)	1.679^{+43}_{-16}	156
2064f21b676m007m050	$20^3 \times 64$	6.76	0.007	0.050	0.8678	2.635(3)	1.672^{+43}_{-16}	200
2064f21b676m010m050	$20^3 \times 64$	6.76	0.010	0.050	0.8677	2.619(3)	1.663^{+43}_{-16}	200
			$a \approx 0.15$ fm					
2048f21b6566m00484m0484	$20^3 \times 48$	6.566	0.00484	0.0484	0.8602	2.162(5)	1.373^{+34}_{-14}	560
1648f21b6572m0097m0484	$16^3 \times 48$	6.572	0.0097	0.0484	0.8604	2.140(4)	1.358^{+35}_{-13}	250
1648f21b6586m0194m0484	$16^3 \times 48$	6.586	0.0194	0.0484	0.8609	2.129(3)	1.352^{+35}_{-13}	200

where a is the s-wave $\pi\pi$ scattering length, r is the effective range, and k is the magnitude of the center-of-mass scattering momentum related to the energy $E^I_{\pi\pi}$ of the $\pi\pi$ system with total isospin I in a torus of size L by

$$k^2 = \frac{1}{4}(E^I_{\pi\pi})^2 - m_\pi^2, \qquad k = \frac{2\pi}{L}q, \tag{5}$$

where the dimensionless momentum $q \in \mathbb{R}$. The s-wave $\pi\pi$ scattering length in the continuum limit is denoted by

$$a_0 = \lim_{k\to 0} \frac{\tan\delta_0(k)}{k},$$

which is purely elastic below inelastic thresholds.[2] We should keep in mind that the truncation of the effective range r in Eq. (4) is considered to be an important source of systematic error, which appears as $\mathcal{O}(1/L^6)$. The $\delta_0(k)$ can be computed by the Lüscher formula [37,38]:

$$k\cot\delta_0(k) = \frac{2\pi}{L}\pi^{-3/2}\mathcal{Z}_{00}(1, q^2), \tag{6}$$

where the dimensionless momentum $q = kL/(2\pi)$ and the zeta function $\mathcal{Z}_{00}(1; q^2)$ is formally expressed by

$$\mathcal{Z}_{00}(1; q^2) = \frac{1}{\sqrt{4\pi}}\sum_{\mathbf{n}\in\mathbb{Z}^3}\frac{1}{n^2 - q^2}. \tag{7}$$

We generally compute the zeta function by the method discussed in Ref. [24]. Recently, an equivalent formula has been established [65]. It allows us to avoid the subthreshold singularities inherent to the Lüscher technique [65].

The energy $E^I_{\pi\pi}$ can be secured from the $\pi\pi$ four-point function which manifests as [66]

$$C^I_{\pi\pi}(t) = Z_{\pi\pi}\cosh\left[E^I_{\pi\pi}\left(t - \frac{1}{2}T\right)\right] + (-1)^t Z'_{\pi\pi}\cosh\left[E^{I\prime}_{\pi\pi}\left(t - \frac{1}{2}T\right)\right] + \cdots. \tag{8}$$

For a large t to reduce the excited states, the terms alternating in sign are a representative feature of a staggered scheme [66], and the ellipsis indicates the contributions from the excited states which are suppressed exponentially. In practice, the pollution due to the "wraparound" effects [21,27,67] should be taken into account.

It should be worthwhile to stress that, even if we project onto the Goldstone pions at source and sink time slices, pions with all 16 staggered flavors still emerge at the intermediate times [17]. However, in large t, the contributions of non-Goldstone pions in the intermediate states are exponentially reduced due to their heavier masses, in contrast with those of the Goldstone pions [17–19].

In practice, for the sake of a more intuitive presentation of our results, we compute the ratios[3]

$$R^X(t) = \frac{C^X_{\pi\pi}(0, 1, t, t+1)}{C_\pi(0, t)C_\pi(1, t+1)}, \qquad X = D, C, R, \text{ and } V, \tag{9}$$

where $C_\pi(0, t)$ and $C_\pi(1, t+1)$ are pion correlators with zero momentum. With the consideration of Eq. (3), we can depict the $\pi\pi$ scattering amplitudes which project out the $I = 0$ and 2 isospin eigenstates as

[2] We are only interested in the elastic region, $2m_\pi < E^I_{\pi\pi} < 4m_\pi$, where there is no 4π channel, and not yet up to the opening of the $K\bar{K}$ channel at around 1 GeV [63], where the $K\bar{K}$ channel contributes remarkably to the isoscalar $\pi\pi$ interactions [64].

[3] In principle, when $t \ll T/2$, even if we place the periodic boundary condition in the temporal direction, the energy shift of the $\pi\pi$ system can still be roughly evaluated from these ratios. In this work, we do not use these ratios to quantitatively calculate any physical quantities; nonetheless, these ratios will indeed help us to qualitatively or intuitively comprehend some physical quantities.

$$R_{I=0}(t) = R^D(t) + \frac{1}{2}N_f R^C(t) - 3N_f R^R(t) + \frac{3}{2}R^V(t),$$
$$R_{I=2}(t) = R^D(t) - N_f R^C(t). \tag{10}$$

In this work, we will employ two approaches to calculate the pion mass m_π. The first method is to use both the point-source and point-sink operators. Nevertheless, the point operator has a big overlap with excited states [68], and in practice it is customary to use the wall-source operator which efficiently reduces these overlaps, along with a point sink [68]. In addition, we need both propagators to calculate the pion decay constant [50,51].

III. LATTICE CALCULATION

We used the MILC gauge configurations [50,51] with the 2 + 1 flavors of Asqtad-improved staggered sea quarks [52] and a Symanzik-improved gluon action [69]. See detailed simulation parameters in Ref. [70]. It is worth mentioning that the MILC gauge configurations are generated using the staggered formulation of lattice fermions [71] with the fourth root of a fermion determinant which is hypercubic smeared (HYP smeared) [72]. As shown in Ref. [73], the chiral symmetry is significantly enhanced via the HYP-smeared gauge link.

The lattice simulation parameters of the MILC gauge configurations used here are epitomized in Table I. The simulated bare masses of light and strange sea quarks are denoted by am_l and am_s, respectively. The masses of the u and d quarks are degenerate and small enough that the physical up- and down-quark masses can be attained by the chiral extrapolation. The lattice spacing a for first three lattice ensembles is about 0.12 fm, and that of the last three lattice ensembles is around 0.15 fm. By MILC convention, the lattice ensembles are referred to as "coarse" for $a \approx 0.12$ fm and "medium coarse" for $a \approx 0.15$ fm. For easy notation, it is convenient to use (am_l, am_s) to mark lattice ensembles, e.g., "the (0.01, 0.05) ensemble." The tadpole factors u_0 [75] are utilized to enhance the gauge configuration action [50,51].

To compute the $\pi\pi$ four-point functions $C_{\pi\pi}(t)$, the standard conjugate gradient technique[4] is used to acquire the required matrix element of the inverse fermion matrix. The periodic boundary condition is applied to the three spatial directions and temporal direction. We compute $C_{\pi\pi}(t)$ on all possible time slices, and collect them at the end of the measurement, namely,

$$C_{\pi\pi}(t) = \frac{1}{T}\sum_{t_s=0}^{T-1}\langle(\pi\pi)(t+t_s)(\pi\pi)^\dagger(t_s)\rangle.$$

After averaging the correlators over all possible T values of common time shift t_s, as illustrated later, we found that the statistics are indeed significantly improved.

For each time slice, three fermion matrix inversions are needed, corresponding to the three color choices for the pion source, and each inversion takes about 1000 iterations [about 2000 for the (0.00484, 0.0484) and (0.005, 0.05) ensembles] during the conjugate gradient calculation. Thus, in total, we carry out $3T$ inversions on a single gauge configuration. As shown later, this rather big number of inversions offers the substantial statistics needed to get the $\pi\pi$ scattering amplitudes with high accuracy.

In practice, we calculate the pion correlators,

$$C_\pi^{\mathrm{PP}}(t) = \frac{1}{T}\sum_{t_s=0}^{T-1}\langle 0|\pi^\dagger(t+t_s)\pi(t_s)|0\rangle,$$
$$C_\pi^{\mathrm{WP}}(t) = \frac{1}{T}\sum_{t_s=0}^{T-1}\langle 0|\pi^\dagger(t+t_s)W_\pi(t_s)|0\rangle, \tag{11}$$

where π is the pion point-source operator and W_π is the pion wall-source operator [50,51]. To simplify the notation in this section, the summation over the lattice space point in sink is not written out. In this work, we will adopt the shorthand notation: "PP" for the point-source point-sink propagators and "WP" for the wall-source point-sink propagators [51]. We should stress that the summations are also taken over all the time slices for the pion propagators, and we found that the statistics are indeed significantly improved. This is very important to obtain a pion mass with high accuracy.

Overlooking the excited state contributions, the pion mass m_π can be secured at large t with a single exponential fit ansatz [61,70,76]

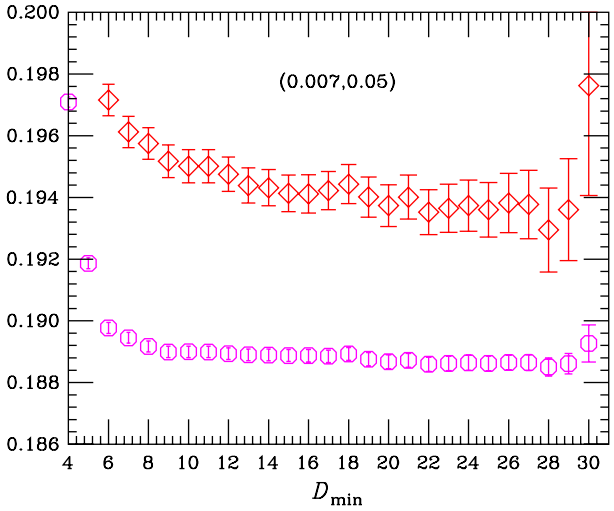

FIG. 2 (color online). Pion masses (magenta octagons) and WP amplitudes A_π^{WP} (red diamonds) as a function of the minimum time distance in the fit for the (0.007, 0.05) ensemble. The amplitudes have been divided by 2060.

[4]The conjugate gradient residual used in this work is 1.0×10^{-5}, which is smaller than that used in generating gauge configurations [50,51]. Moreover, to avoid the potential roundoff errors as much as possible, all of the numerical calculations are calculated in double precision.

TABLE II. Summaries of the pion masses and pion decay constants. The third column shows the pion masses in lattice units and the fifth column gives the overlapping amplitude using WP propagators. The product of $m_\pi L$ is presented in column 4. The pion decay constants in lattice units are provided in the sixth column. Column 2 shows the values of pion mass in MeV, where the errors are estimated from both the error on lattice spacing a and statistical errors in column 3. The seventh column shows the dimensionless ratio m_π/f_π, where the errors are estimated from the am_π and af_π. The last column shows the pion masses which are measured by the point-wall point-sink propagators, and only used as a consistency check.

Ensemble	m_π (MeV)	am_π^{WP}	$m_\pi^{\mathrm{WP}}L$	A_π^{WP}	af_π	m_π/f_π	am_π^{PP}
(0.00484, 0.0484)	240(4)	0.17503(09)	3.5006(18)	1000.18 ± 1.580	0.11767(45)	1.4874(57)	0.17504(09)
(0.005, 0.05)	268(5)	0.15970(15)	3.8345(48)	770.534 ± 2.577	0.09054(33)[a]	1.7639(66)	0.15992(16)
(0.007, 0.05)	315(6)	0.18868(22)	3.7736(44)	399.094 ± 1.393	0.09364(20)[a]	2.0149(49)	0.18871(24)
(0.0097, 0.0484)	334(6)	0.24566(18)	3.9306(29)	395.107 ± 1.151	0.12136(29)	2.0242(51)	0.24587(21)
(0.01, 0.05)	373(7)	0.22455(27)	4.4910(54)	365.595 ± 2.039	0.09805(14)[a]	2.2902(42)	0.22447(17)
(0.0194, 0.0484)	463(8)	0.34279(19)	5.4846(30)	315.695 ± 0.865	0.13055(48)	2.6258(98)	0.34279(23)

[a]The superscript indicates the MILC's determination.

$$C_\pi^{\mathrm{PP}}(t) = A_\pi^{\mathrm{PP}}[e^{-m_\pi t} + e^{-m_\pi(T-t)}], \tag{12}$$

$$C_\pi^{\mathrm{WP}}(t) = A_\pi^{\mathrm{WP}}[e^{-m_\pi t} + e^{-m_\pi(T-t)}], \tag{13}$$

where T is the temporal extent of the lattice, and A_π^{PP} and A_π^{WP} are overlapping amplitudes. We will use these values to estimate the wraparound contributions [21,27,67] and calculate the pion decay constant [68] as well.

We should remark at this point that, in the calculation of the $\pi\pi$ four-point functions for the $I = 0$ channel, we try our best to compute the vacuum diagram, since the other three diagrams can be relatively easily calculated. We found that the vacuum diagram plays a critical role in this correlator.[5]

IV. LATTICE SIMULATION RESULTS

A. Pion mass and pion decay constant

In practice, the π propagators were fit by varying minimum fitting distances $\mathrm{D_{min}}$ and by putting the maximum distance $\mathrm{D_{max}}$ either at $T/2$ or where the fractional statistical errors surpassed about 20% for two sequential time slices [50,51,61].[6] In this work, pion masses were secured from the "effective mass" plots for each of the MILC lattice ensembles, and they were strenuously selected by looking for a combination of a "plateau" in the mass as a function of $\mathrm{D_{min}}$, good fit quality (i.e., $\chi^2/\mathrm{d.o.f.} \leq 1$), and $\mathrm{D_{min}}$ large enough to reduce the excited states [25–27]. The WP propagators were fit to Eq. (13) using a minimum time distance of $14a$ for the medium-coarse lattices and $20a$ for the coarse lattices, and the full covariance matrix is used to compute statistical errors. At these large distances, the pollution from excited states is at most comparable to the statistical errors [68]. For example, Fig. 2 exhibits the results for pion masses and amplitudes as a function of $\mathrm{D_{min}}$ for the (0.007, 0.05) ensemble. Since the major objective of this work is to present the work for isospin-0, as explained later, for $\pi\pi$ scattering in the $I = 0$ channel, the systematic error of the energy of the $\pi\pi$ system is fairly large; we can temporarily neglect the systematic effect for pion mass due to excited states. All of these fitted values of pion masses are listed in Table II.

In our previous work [33], we used the method described in Ref. [68] to extract the pion decay constant for the (0.0097, 0.0484) ensemble [33]. In light of the same procedures, we calculated the pion decay constants for other medium-coarse ensembles. All of these fitted values of pion decay constants are listed in Table II.

As a consistency check, the PP correlators were reliably measured in this work. Using these correlators, we can secure pion masses via Eq. (12), which are listed in the last column in Table II, and these pion masses are found to be consistent with their counterparts extracted with WP propagators, which are summarized in Table II.

Our fitted values of pion masses and pion decay constants listed in Table II are in rather good agreement with the same quantities which are computed on the same lattice ensembles by the MILC Collaboration in Refs. [70,76]. For the coarse ensembles, the MILC's determinations on pion decay constants are directly quoted [70,76], which are also summarized in Table II.

B. Diagrams *D*, *C*, *R*, and *V*

As practiced in our former work [33], the $\pi\pi$ four-point functions are robustly calculated on six MILC lattice ensembles listed in Table I using the technique of the moving wall source without gauge fixing [18,19,53]. In Fig. 3, the

[5]In our previous work [77], we presented a detailed procedure to calculate the disconnected diagram for the $f_0(600)$ meson. It helps us greatly to implement the evaluation of the vacuum diagram here, especially for conducting a vacuum subtraction.

[6]Since the lattice data points at the largest distances contain relatively little information, the exact selection of large distance cutoff $\mathrm{D_{max}}$ is not very critical [50,51,61].

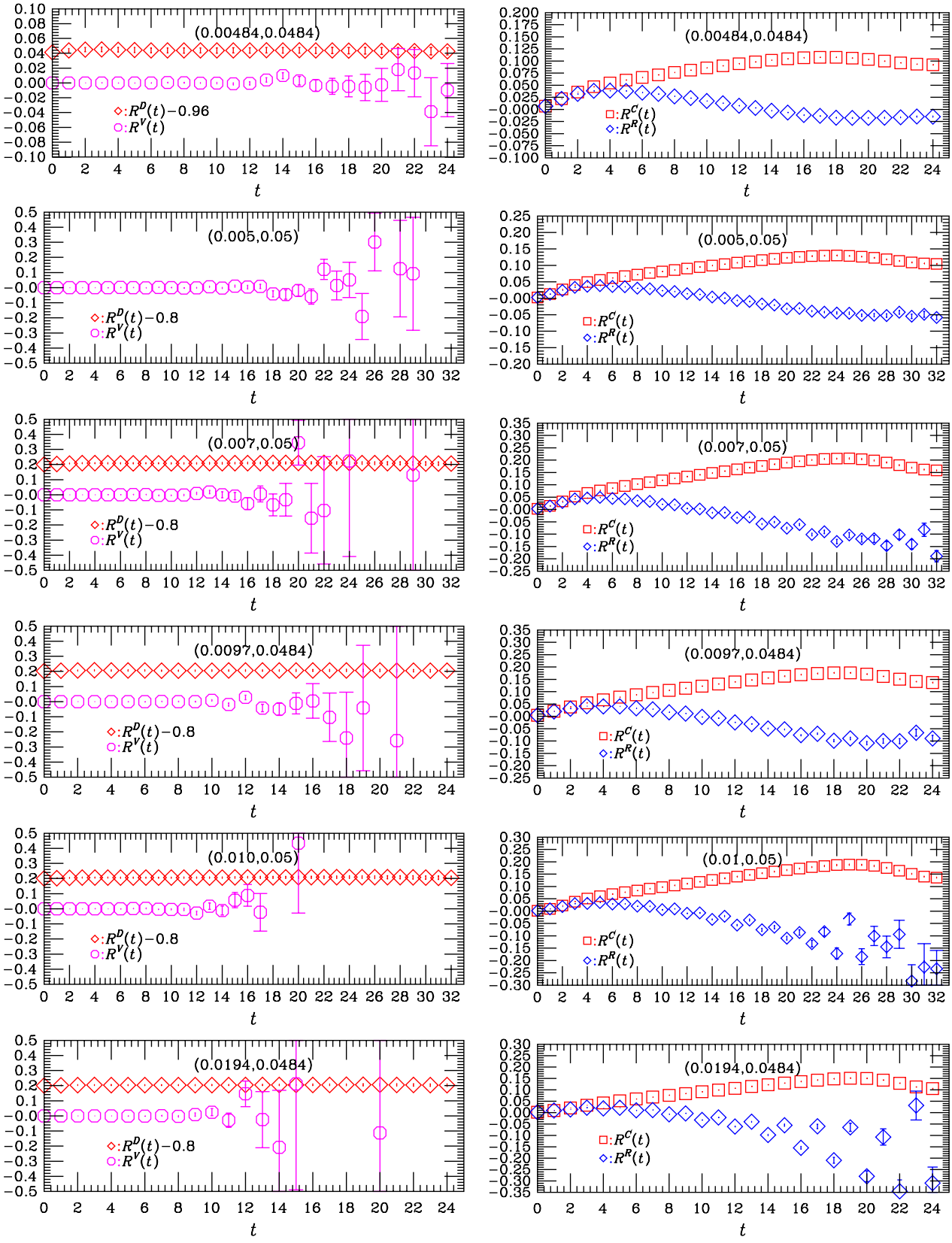

FIG. 3 (color online). Individual amplitude ratios $R^X(t)$ of the $\pi\pi$ four-point functions computed via the moving wall source without gauge fixing as the functions of t for six MILC lattice ensembles: direct diagram (red diamonds) displaced by 0.8 [except for the (0.00484, 0.0484) ensemble, where the direct diagram shifted by 0.95], vacuum diagram (magenta octagons), crossed diagram (red squares), and rectangular diagram (blue diamonds).

individual ratios $R^X(X = D,\ C,\ R,$ and $V)$, which are denoted in Eq. (9), are illustrated as the functions of t for each lattice ensemble.

The ratio values of the direct amplitude R^D are quite close to oneness, indicating a fairly weak interaction in this channel. The crossed amplitude, in another aspect, increases linearly up to $t \sim 18$ for the medium-coarse ensemble and $t \sim 24$ for the coarse ensemble, implying a repulsive interaction between two pions in the $I = 2$ channel. In contrast, after a beginning increase up until $t \sim 4$, the rectangular amplitude demonstrates a roughly linear decrease up until $t \sim 18$ for the medium-coarse ensemble and $t \sim 24$ for the coarse ensemble, suggesting an attractive force among two pions for the $I = 0$ channel. Additionally, the magnitude of the slope is similar to that of the crossed amplitude but with opposite sign. Furthermore, we observe that the crossed and rectangular amplitudes have the same values at $t = 0$ and close ones for small t. These characteristics are in good keeping with the theoretical predictions [17].

For the vacuum amplitude of the (0.0194, 0.0484) ensemble, we only obtain a good signal up to $t = 10$, beyond which signals are quickly lost. For the lattice ensembles with the pion mass becoming smaller, the signals of the vacuum amplitude are lost more slowly. Moreover, for the (0.00484, 0.0484) ensemble, good signals can be observed up to $t = 20$ for the vacuum amplitude. These characteristics are in good accordance with the empirical Okubo-Zweig-Iizuka (OZI) rule and χPT which expect the disappearance of the vacuum amplitude in leading order [17–19]. Additionally, this qualitatively confirmed the analytical arguments in Ref. [34], which indicates that the error of the vacuum amplitude grows exponentially as $e^{2m_\pi t}$. The numerical calculation of the amplitude for the vacuum diagram stands as our principal and distinctive accomplishment of this paper.

The systematically oscillating behavior of the rectangular amplitude in large t is evidently observed, which is a typical feature of the staggered formulation of lattice fermions and corresponds to the contributions from the intermediate states with opposite parity [66], and for the lattice ensemble with large pion mass, this oscillating feature become more obvious. In contrast, for that with small pion mass, this feature is not appreciable, and not even perceptible for the MILC (0.00484, 0.0484) ensemble. The physical meaning of this fascinatingly oscillating behavior is easily understood [66]. Nevertheless, its quantitative mass dependence is not clear to us and needs further investigation.

C. The errors of $R^V(t)$ and $R^R(t)$

According to the analytical arguments in Ref. [34], the error of the ratio for the vacuum amplitude increases exponentially as $e^{2m_\pi t}$. Therefore, it is fairly difficult to secure the correct signal for large t [34]. Likewise, the ratio for the rectangular diagram has errors, which grow exponentially as $e^{m_\pi t}$ for large t [34]. Our lattice data indeed demonstrate such dependence with the expected slopes.

The magnitudes of these errors are quantitatively in line with these analytical predictions, as demonstrated in Fig. 4. Fitting the errors $\delta R^V(t)$ and $\delta R^R(t)$ by a single exponential fit ansatz $\delta R^V(t) \sim e^{\mu_V t}$ and $\delta R^R(t) \sim e^{\mu_R t}$, respectively, for six lattice ensembles, we extract the fitted values of μ_V and μ_R, which are summarized in Table III, together with their fitting ranges.

From Table III, we note that the fitted values of μ_R can be compared with the pion masses m_π listed in Table II, and half of the fitted values of μ_V can also be reasonably compared with these pion masses. Here we have numerically confirmed Lepage's analytical arguments [34] about

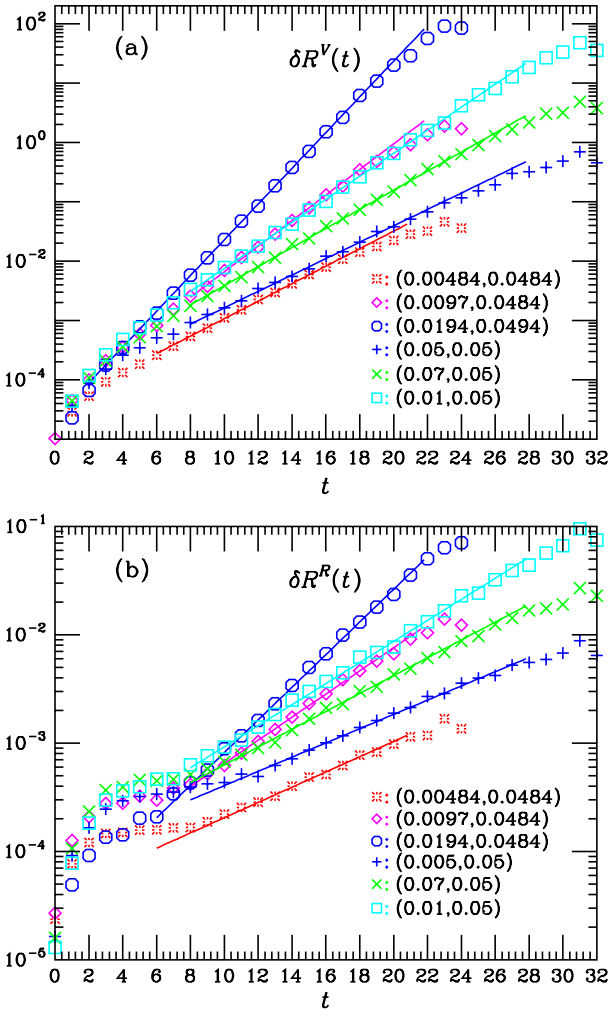

FIG. 4 (color online). The errors of the amplitude ratios $R^X(t)$ $(X = V, R)$ as the functions of t for each of the MILC lattice ensembles. Solid lines are single exponential fits, and the fitting ranges are listed in Table III. (a) The errors of the amplitude ratios $R^V(t)$. (b) Those of $R^R(t)$.

TABLE III. Summaries of the fitted values for μ_V and μ_R in lattice units. The second and third columns show the fitted values of μ_V and μ_R, respectively, and column 4 gives the time range for the chosen fit.

Ensemble	$a\mu_V$	$a\mu_R$	Range
(0.00484, 0.0484)	0.3392	0.1621	10–18
(0.0097, 0.0484)	0.4956	0.2457	8–16
(0.0194, 0.0484)	0.6927	0.3487	8–16
(0.005, 0.05)	0.3178	0.1513	10–20
(0.007, 0.05)	0.3701	0.1895	10–20
(0.01, 0.05)	0.4463	0.2237	10–20

$\pi\pi$ scattering. This testifies to the practical applicability of the moving wall source without gauge fixing from another point of view. Thus, we can reasonably assume that the vacuum amplitude remains small for large t. In principle, we can overlook the vacuum amplitude in the rest of the analysis. However, we will explicitly include it for the sake of completeness of the lattice QCD calculation.

D. R_I projected onto the $I = 0$ and 2 channels

The ratios $R_I(t)$ projected onto the isospin $I = 0$ and 2 eigenchannels for the MILC (0.00484, 0.0484) and (0.005, 0.05) ensembles are demonstrated in Fig. 5. A decrease of the ratio $R_{I=2}(t)$ indicates a repulsive interaction among two pions for the $I = 2$ channel; on the other hand, an increase of the ratio $R_{I=0}(t)$ suggests an attractive interaction for the $I = 0$ channel. In the $I = 0$ channel, a dip at $t = 3$ for (0.00484, 0.0484) and $t = 5$ for (0.005, 0.05) can be clearly observed, and their physical origin is not clear to us as well [18,19].

Due to the rather small quark mass of two lattice ensembles, the systematically oscillating behavior for the $I = 0$ channel in large t is not clearly observed, which is a typical characteristic of the Kogut-Susskind formulation of lattice fermions [66]. Additionally, this oscillating feature is hardly noticed for the $I = 2$ channel.

In order to present the contribution from the vacuum term more intuitively, we employ the green cross points to indicate the ratio $R_I(t)$ for the $\pi\pi$ four-point function in the $I = 0$ channel without the presence of the disconnected diagram. From Fig. 5, we can clearly notice that the contribution from the disconnected diagram is only obvious when $t \geq 20$ for the (0.00484, 0.0484) ensemble and $t \geq 16$ for the (0.005, 0.05) ensemble.

E. Lattice artifact

From Fig. 3, we observe that there exists a pollution from the wraparound effects [21,27,67], approximately starting as early as at $t = 12$–18 for the MILC medium-coarse ensembles and $t = 22$–25 for the coarse ensembles. As discussed in Refs. [21,27,31,67], one of two pions can

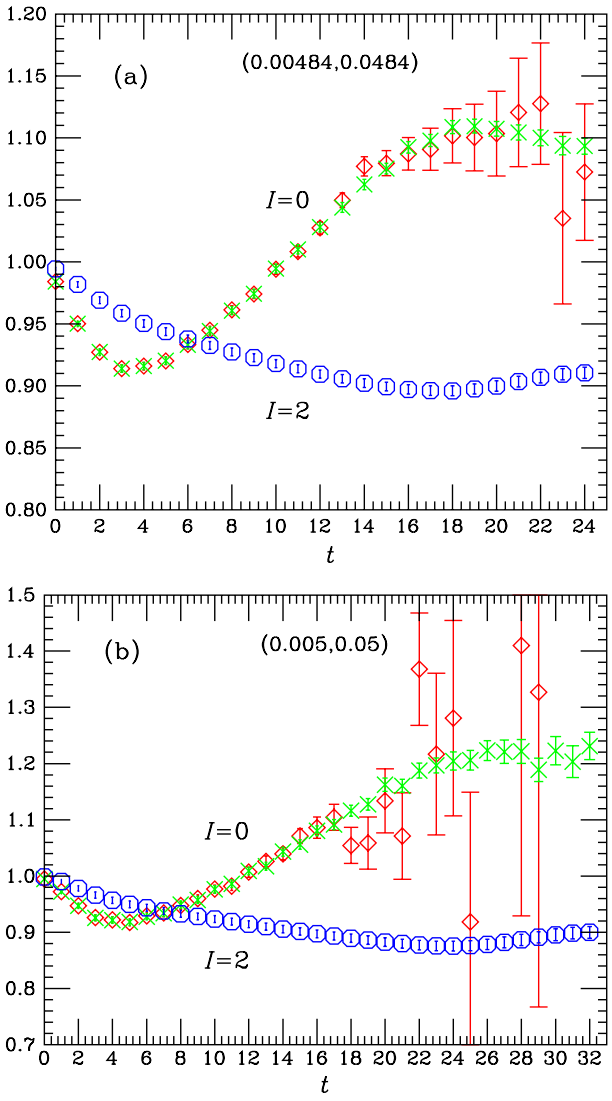

FIG. 5 (color online). $R_I(t)$ ($I = 0$ and 2) for the $\pi\pi$ four-point function at zero momenta calculated by the moving wall source without gauge fixing as the functions of t for the MILC lattice (a) (0.00484, 0.0484) ensemble and (b) (0.005, 0.05) ensemble. The green cross points indicate the ratio $R_I(t)$ in the $I = 0$ channel where the vacuum diagram is turned off.

propagate $T - t$ time steps backwards due to the periodic boundary condition in the temporal direction. This operates as a constant contribution and deforms the $\pi\pi$ four-point functions in large t (especially around $T/2$); according to the discussions in Refs. [21,27,31,67], it is roughly suppressed by

$$\exp(-m_\pi T)/\exp(-2m_\pi t),$$

as compared to forward propagation of the $\pi\pi$ state. We can select the fitting ranges satisfying $t_{\max} \ll T/2$ to reduce this effect [21]. However, according to the arguments in Refs. [21,27,31,67], if pion mass is small enough [e.g., the (0.00484, 0.0484) ensemble], the wraparound

TABLE IV. Summaries of the calculated wraparound contributions from overlapping amplitude A_π and pion mass am_π. The second column shows the wraparound contributions calculated from Eq. (15), where its errors are roughly estimated from the statistical errors of A_π and m_π.

Ensemble	C
(0.00484, 0.0484)	451.36(2.63)
(0.005, 0.05)	43.23(51)
(0.007, 0.05)	1.815(29)
(0.0097, 0.0484)	2.362(25)
(0.01, 0.05)	0.1533(31)
(0.0194, 0.0484)	0.01424(15)

pollution cannot be suppressed even for $t \ll T/2$; we should include this term for the successful fit,[7]

$$C^I_{\pi\pi}(t) = C + A_{\pi\pi}\cosh\left[E^I_{\pi\pi}\left(t-\frac{1}{2}T\right)\right] + (-1)^t A'_{\pi\pi}\cosh\left[E^{I\prime}_{\pi\pi}\left(t-\frac{1}{2}T\right)\right] + \cdots, \quad (14)$$

where C is a constant corresponding to the wraparound term. This can be easily understood by evaluating the contribution of two fake diagrams in Fig. 2 of Ref. [31], and C can be expressed as

$$C = 2A_\pi^2 e^{-m_\pi T}. \quad (15)$$

For easy notation, the superscript WP in A_π is omitted in the rest of our analyses.

In this work, we accurately extract the overlapping amplitudes A_π and pion masses m_π corresponding to pion correlators [78], which are listed in Table II, and these values are sufficiently precise to estimate the wraparound terms with Eq. (15), which are listed in Table IV.

We note that Ref. [30] has recently taken the similar definition as

$$C = 2A_{\pi\pi}e^{-m_\pi T}, \quad (16)$$

where $A_{\pi\pi}$ is defined in Eq. (14). Additionally, there exists the similar general form which contains the two-particle, as well as one-particle, eigenvalues and gives a not-quite rigorous proof in Ref. [79]. Furthermore, when studying $K \to \pi\pi$ decay amplitudes, there is an analogous fitting functional form in Ref. [56].

In order to comprehend these wraparound effects at a quantitative level, we denote a quantity

$$R_{WC}(t) = \frac{C}{C^{I=2}_{\pi\pi}(t)}, \quad (17)$$

[7]It turns out that a five-parameter cosh fit of $C, A_{\pi\pi}, E^I_{\pi\pi}, A'_{\pi\pi}$, and $E^{I\prime}_{\pi\pi}$ yields a satisfactory result with a fairly acceptable χ^2. Moreover, the excited states will be taken into account as one of the important sources of systematical error in this work.

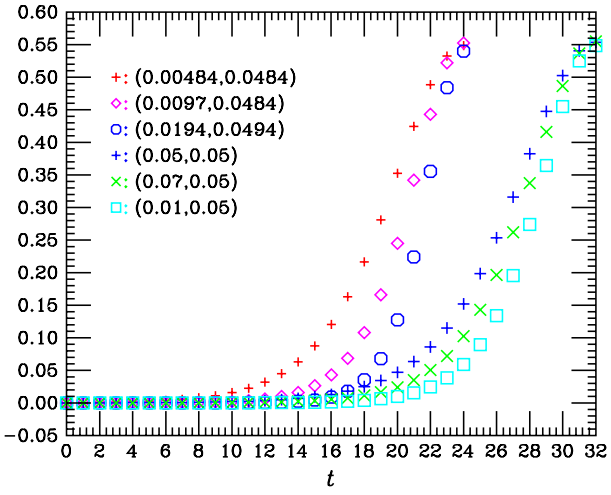

FIG. 6 (color online). The ratios of the wraparound terms to the corresponding $\pi\pi$ four-point functions for six MILC lattice ensembles calculated by Eq. (17). All of these ratios make a significant contribution and are approximately close to $1/2$ as t approaches to $T/2$, as expected from the arguments in Refs. [21,27,31,67].

which is the ratio of the wraparound pollution to the $\pi\pi$ four-point function in the $I = 2$ channel. In fact, we exploited the data of the wraparound contribution C listed in Table IV and $C^{I=2}_{\pi\pi}(t)$ calculated from Eq. (3) to approximately evaluate these ratios. The ratios for six MILC lattice ensembles are illustrated in Fig. 6. All of these ratios make a significant contribution and are approximately close to $1/2$ as t approaches to $T/2$, as expected from the arguments in Refs. [21,27,31,67]. We can note that as the pion mass of the lattice ensemble becomes smaller, the wraparound contribution C is clearly observed even at small t. For example, we can keenly notice the wraparound term even as early as at $t = 10$–12, satisfying $t \ll T/2$ for the (0.00484, 0.0484) ensemble. It is, therefore, absolutely necessary for us to explicitly consider the wraparound term, especially for lattice ensembles with small pion masses when we extract the energy E of the $\pi\pi$ system [31].

To get rid of this pollution, Xu *et al.* [27] employed a derivative method and denoted a modified ratio [67]. By ignoring terms suppressed relative to the leading contribution, the energy shift δE can be obtained from the asymptotic form of the modified ratio. To identify the time separations where the ground state dominates, Yagi *et al.* used their self-defined ratios [31]. Moreover, Dudek *et al.* [30] recently eliminated this unwanted pollution term by the shifted correlator.

In principle, we can use one of the three above-mentioned methods to process our $\pi\pi$ scattering data for isospin-2. However, for those of the $I = 0$ channel, there is a further complication introduced by staggered fermions: the oscillating term is appreciable, so we must consider the oscillating term and modify the corresponding functional

forms. As a consequence, it is not convenient to use these methods. Additionally, for pion-kaon (πK) scattering [53,78] and the $\pi\pi$ correlators "in flight" [30], the wraparound term is not a constant, and these methods are not suitable.

Nagata *et al.* solved this problem by subtracting the wraparound term numerically from the obtained quantities [78], since the lattice-measured data are sufficiently precise to allow such subtraction. Dudek *et al.* eliminated this term by means of the shifted correlator for $\pi\pi$ scattering at rest and the weight-shifted correlator for $\pi\pi$ scattering in flight [30]. We already exhibited that the overlapping amplitude A_π and pion mass m_π can be calculated with high accuracy, so it is natural to borrow these methods for our case [30,78]. As a consistency check, we numerically compared these results calculated from the above-mentioned methods for lattice data in the $I = 2$ channel, and we found that they are consistent with each other within errors. Therefore, in this work we only present the results from the last method, namely, using Eq. (14) to extract the energy E of the $\pi\pi$ system in a conceptually clean way.

V. FITTING ANALYSES

As already explained in previous sections, we will use Eq. (14) to get the energies aE of the $\pi\pi$ system, which are inserted into the Lüscher formula (6) to obtain the corresponding s-wave $\pi\pi$ scattering lengths. Hence, appropriately extracting the energies is a central step toward our ultimate results. A persuasive way to process our lattice data is to resort to the "effective energy" plot, which is a variant of the effective mass plot, and very similar to the "effective scattering length" plot [25,26].

A. $I = 2$ channel

In practice, $\pi\pi$ four-point functions were fit by varying the minimum fitting distances $\mathrm{D_{min}}$ and by putting the maximum distance $\mathrm{D_{max}}$ either at $T/2$ or where the fractional statistical errors surpassed about 20% for two sequential time slices [50,51,61]. Additionally, the fitting parameter C was constrained by priors to conform to the lattice-calculated wraparound contribution C listed in Table IV [80]. For each ensemble, the effective energy plots as a function of $\mathrm{D_{min}}$ are illustrated in Fig. 7. The central value and statistical error at each time slice were evaluated by the Levenberg-Marquardt algorithm [81]. To make these fits more robust, we double-check them with SNOBFIT, which is a soft constrained noisy optimization [82]. From Fig. 7, we also observed that the effective energies have larger statistical errors near $t \sim T/2$ because of the wraparound effect, as discussed in detail in Ref. [31].

In this work, the energies aE of the $\pi\pi$ system in the $I = 2$ channel were secured from the effective energy plots for each of the MILC lattice ensembles, and they were strenuously selected by looking for a combination of the plateau in the energy as the function of $\mathrm{D_{min}}$, good fit quality [25–27], and $\mathrm{D_{min}}$ large enough to suppress the excited states. We found that the effective energy of the $\pi\pi$ system for the $I = 2$ channel has relatively small errors within a broad minimum time distance region.

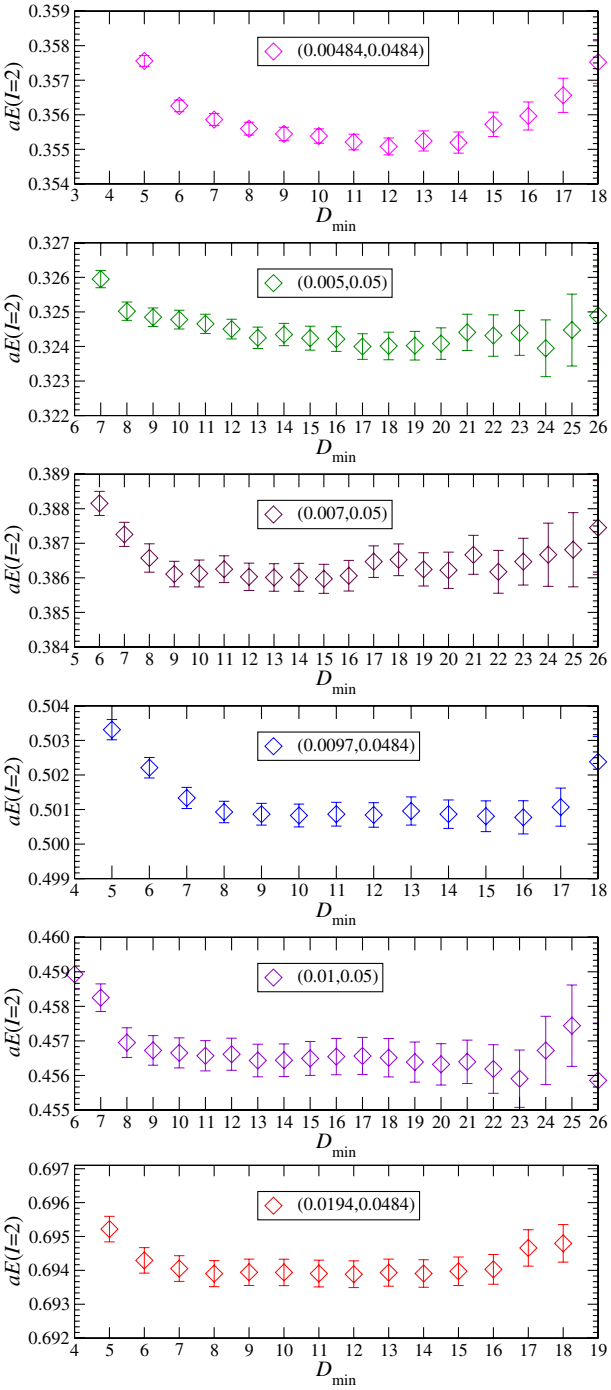

FIG. 7 (color online). The effective energy plots as the functions of $\mathrm{D_{min}}$ for $\pi\pi$ scattering in the $I = 2$ channel in lattice units. The effective energy plots have small errors within a broad minimum fitting distance region.

We should remark that the physical model in Eq. (14) just includes the ground state [25–27]. In fact, we can fit with the inclusion of the first excited state, and the

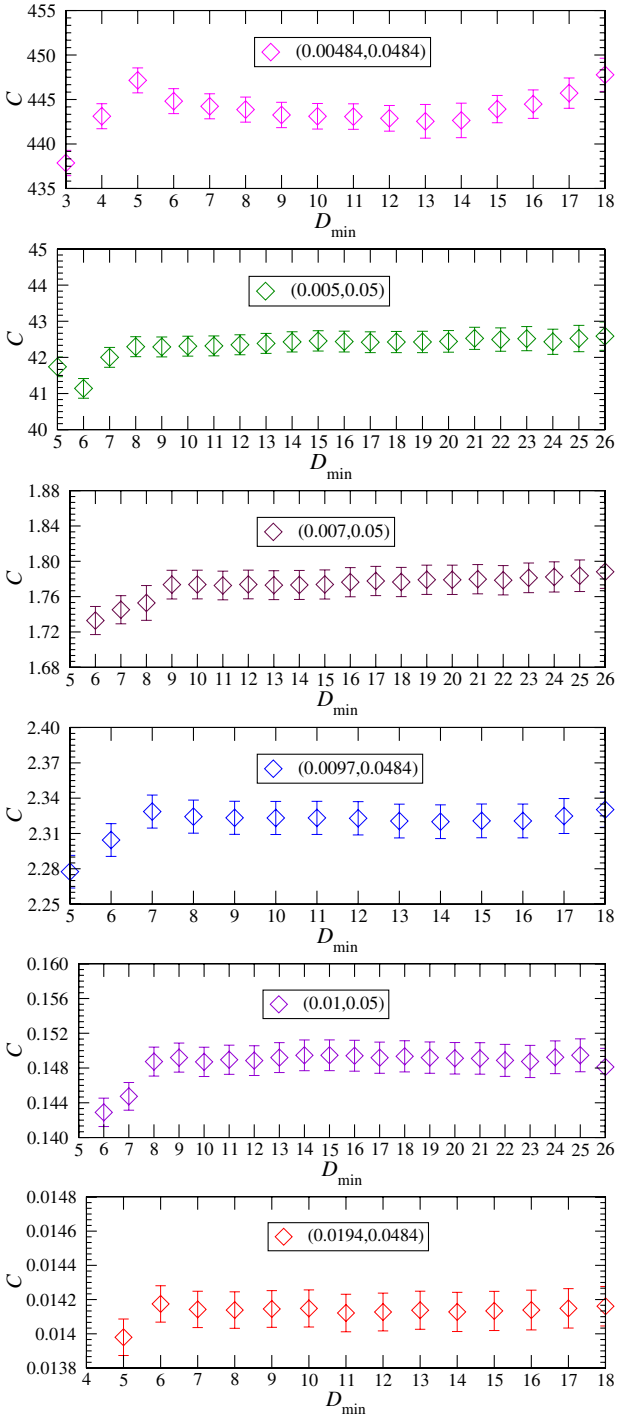

FIG. 8 (color online). The effective wraparound constant plots as the functions of D_{min} for $\pi\pi$ scattering in the $I = 2$ channel in lattice units.

difference between these procedures, as well as the difference arising from the arbitrary choice of D_{max}, is incorporated in the systematic error for the energies aE of the $\pi\pi$ system.

For the same fitting range, analogously, we secured the wraparound term C from the corresponding effective wraparound constant plots in Fig. 8. It is worth mentioning that the fitted wraparound pollution C is in fair agreement with the calculated wraparound pollution C within errors. Nonetheless, it is interesting to note that there exist differences of about 1%; the physical indication is not clear to us and needs further investigation in future work.

The fitted values of the energies aE of the $\pi\pi$ system with isospin-2, fitting range, and fit quality (χ^2/d.o.f.) are tabulated in Table V, together with the fitted values of the wraparound contribution C. We note that the fitted values of C are de facto statistically significant constant terms for the lattice ensembles with small pion masses. Additionally, we clearly found that these fitted values of C are close to our estimated values listed in Table IV, as already noticed in Ref. [30].

It is well known that the interaction between two pions in the $I = 2$ channel is fairly weak, such that the energy difference between the interacting and noninteracting $\pi\pi$ states is quite a small fraction of the total energy of the $\pi\pi$ system,[8] which can be estimated from the data in Tables II and V. This forces us to make the rigorous measurements of both the energy spectra of the $\pi\pi$ system and pion masses, and even to seriously account for various small systematic effects to resolve the rather small differences. We have indeed extracted the energies of the $\pi\pi$ system and pion masses with significantly high precision. These are shown in Tables II and V.

Now it is straightforward to substitute these energies aE into Lüscher formula (6) and secure the relevant s-wave scattering lengths $a_{\pi\pi}^{I=2}$, where we plugged in the pion masses from column 3 in Table II. The center-of-mass scattering momentum k^2 is computed by Eq. (5) with pion masses given in Table II. However, to get rid of the scale-setting uncertainties, it turns out to be more customary to adopt the dimensionless quantity: $m_\pi a_{\pi\pi}^{I=2}$ [25,26]. All of these values for each lattice ensemble are summarized in Table V, where the statistical errors of k^2 are calculated from the statistical errors of aE and am_π, and its systematic errors are only estimated from the systematic errors of aE. Likewise, the statistical errors for $m_\pi a_{\pi\pi}^{I=2}$ are computed from the systematic errors of k^2 and am_π, while its systematic errors are estimated from the systematic errors of k^2 and the subsequently mentioned two finite volume effects.

Since the periodic boundary condition is imposed in the spacial directions of the lattice, there is an exponentially small finite volume (FV) correction to the s-wave $\pi\pi$ scattering length in the $I = 2$ channel, which has been determined in the vicinity of the threshold in Ref. [83]. The consequent finite volume correction Δ_{FV} is provided here as [83],

[8]In this work, the ratio of the energy shift to total energy is about 2%. For other lattice studies [17–31], it is actually close to this number. On the other hand, this ratio for the $I = 0$ channel is around 5% [18,19,32], and the ratio of this work is approximately 5% as well.

TABLE V. Summaries of lattice results of the s-wave scattering lengths for the $I = 2$ channel. The second column presents the energies in lattice units, where the first uncertainties are statistical and the second ones are the estimates of the systematic uncertainties due to fitting. Column 3 shows the fitted values of the wraparound term C, column 4 indicates the time range for the chosen fit, and column 5 gives the fit quality χ^2/d.o.f. Column 7 gives the center-of-mass scattering momentum k^2 in GeV, and column 8 presents the product of the pion mass and scattering length, $m_\pi a_{\pi\pi}^{I=2}$, where the first uncertainty is statistical and the second one is systematic.

Ensemble	aE	C	Range	χ^2/d.o.f.	k^2 [GeV^2]	$m_\pi a_{\pi\pi}^{I=2}$
(0.00484, 0.0484)	0.35520(25)(20)	438.05(1.94)	14–24	4.21/6	0.00167(10)(7)	−0.0915(52)(35)
(0.005, 0.05)	0.32424(35)(33)	42.44(29)	16–32	10.6/12	0.00220(21)(15)	−0.125(11)(8)
(0.007, 0.05)	0.38606(44)(37)	1.776(17)	16–32	11.5/12	0.00444(31)(20)	−0.167(10)(7)
(0.0097, 0.0484)	0.50087(41)(38)	2.320(14)	14–24	6.1/6	0.00437(25)(17)	−0.167(9)(6)
(0.01, 0.05)	0.45648(56)(41)	0.1493(18)	18–32	8.7/10	0.00464(48)(26)	−0.209(19)(10)
(0.0194, 0.0484)	0.69392(40)(34)	0.01414(11)	13–24	6.6/7	0.00527(35)(22)	−0.277(16)(10)

$$(m_\pi a_{\pi\pi}^{I=2})_L = (m_\pi a_{\pi\pi}^{I=2})_\infty + \Delta_{\mathrm{FV}}, \tag{18}$$

where

$$\Delta_{\mathrm{FV}} = \frac{1}{2^{13/2}\pi^{5/2}}\left(\frac{m_\pi}{f_\pi}\right)^4 \sum_{\mathbf{n}\in\mathbb{Z}^3}{}' \frac{e^{-|\mathbf{n}|m_\pi L}}{\sqrt{|\mathbf{n}|m_\pi L}}\left\{1 - \frac{17}{8}\frac{1}{|\mathbf{n}|m_\pi L} + \frac{169}{128}\frac{1}{|\mathbf{n}|^2 m_\pi^2 L^2} + \mathcal{O}(L^{-3})\right\}. \tag{19}$$

Here $\sum_{\mathbf{n}\in\mathbb{Z}^3}{}'$ indicates a summation without $\mathbf{n} = \mathbf{0}$. Using this formula, we compute the finite volume corrections to $m_\pi a_{\pi\pi}^{I=2}$, which are listed in Table VI, where we insert the values of $m_\pi L$ and m_π/f_π listed in Table II.

From Table VI, we note that these corrections are more and more important for the lattice ensembles with smaller and smaller pion masses [83]. Since we use the lattice ensembles with small pion masses, we should consider these effects, although they are slight, and never more than 7% of the corresponding statistical errors [27].

Another important finite volume effect stems from effective range approximation, $k\cot\delta(k) = 1/a_{\pi\pi}^{I=2} + \frac{1}{2}rk^2$ [26]. While the dependence on the effective range r is small, the range truncation actually leads to the correction at $O(L^{-6})$ in Lüscher formula (6) [26]. In practice, we compute this correction for each lattice ensemble, as suggested in Ref. [26].

These two finite volume corrections have also been added in quadrature to the systematical errors listed in Table V. Other sources of systematic uncertainty such as isospin violation, finite volume effect due to the fixed global topology, pion mass correction [26,31], etc. are believed to be very small, or we currently do not have enough computational resources to fulfill them. These effects should be incorporated into the more sophisticated lattice computation at some point in the future.

TABLE VI. Summaries of the finite volume corrections Δ_{FV}. Column 2 shows the finite volume corrections to the $I = 2$ $\pi\pi$ scattering length, and column 3 gives ratios of the finite volume corrections to the corresponding statistical error. Here we use the pion masses, pion decay constants, and $m_\pi L$ values listed in Table II.

Ensemble	Δ_{FV}	Ratios
(0.00484, 0.0484)	0.000258	0.049
(0.005, 0.05)	0.000341	0.031
(0.007, 0.05)	0.000625	0.060
(0.0097, 0.0484)	0.000529	0.062
(0.01, 0.05)	0.000453	0.023
(0.0194, 0.0484)	0.000257	0.016

B. $I = 0$ channel

As already performed for the $I = 2$ channel, we analyze our lattice data with the effective energy plot. We should stress that when using physical fitting model (14) to extract the desired energies aE of the $\pi\pi$ system, we fix the fitting parameters of wraparound contribution C with the estimated values listed in Table IV.[9] In practice, the $\pi\pi$ four-point functions were fit by altering the minimum fitting distances $\mathrm{D_{min}}$ and putting the maximum distance $\mathrm{D_{max}}$ either at $T/2$ or where the fractional statistical errors exceeded about 20% for two sequential time slices [50,61]. The effective energy plots as the functions of $\mathrm{D_{min}}$ are illustrated in Fig. 9. The central value and statistical error at each time slice were evaluated by the Levenberg-Marquardt method [81]. To make these fits robust, we double-check them with SNOBFIT [82]. We do not show the result of the (0.0194, 0.0484) ensemble in Fig. 9 since it is too noisy.

For each lattice ensemble, the energies aE of the $\pi\pi$ system for the $I = 0$ channel are secured from the effective energy plots and chosen by looking for a combination of a plateau in the energy as the function of $\mathrm{D_{min}}$, a good confidence level, and $\mathrm{D_{min}}$ large enough to suppress the excited states [25–27]. In addition, as performed for

[9]For rectangular (R) and vacuum (V) diagrams, there is no wraparound pollution. So the wraparound contribution for the $I = 0$ channel is the same as that in the $I = 2$ channel. It is reasonable to fix the wraparound contribution C.

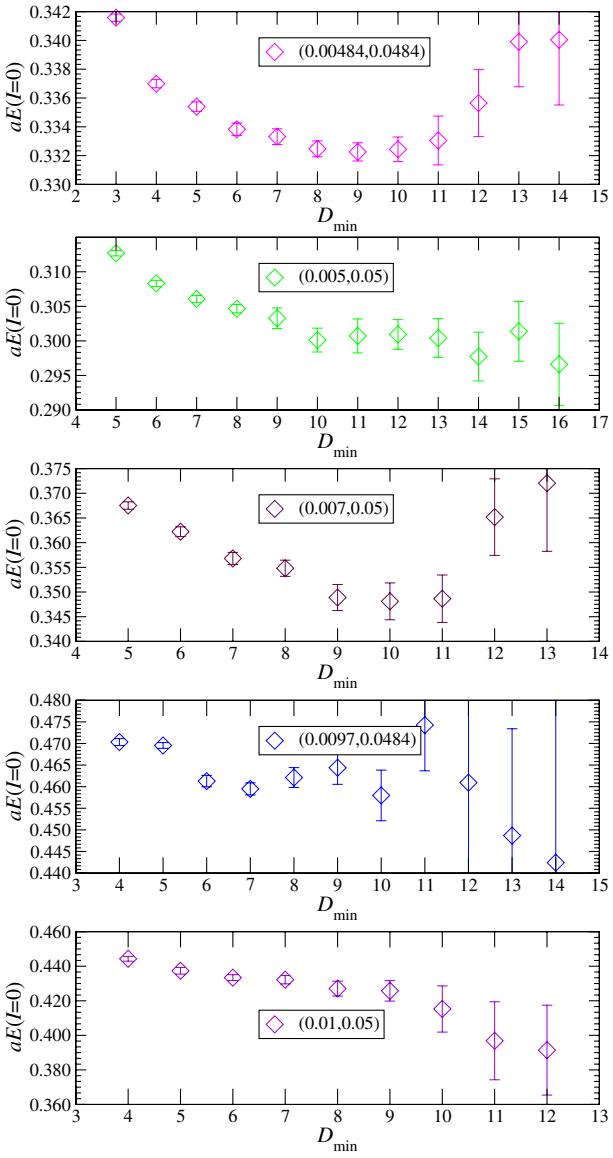

FIG. 9 (color online). Effective energy plots as the functions of D_{min} for $\pi\pi$ scattering in the $I = 0$ channel in lattice units.

isospin-2, we approximately estimate the systematic errors owed to fitting [25–27].

The fitted values of the energies aE of the $\pi\pi$ system, fit range, and fit quality (χ^2/d.o.f.) are summarized in Table VII. The fit quality χ^2/d.o.f. is reasonable for the $I = 0$ channel. It is well known that the disconnected term gives rise to the considerable fluctuations in the $\pi\pi$ four-point function, and it is fairly difficult to reliably calculate this term. In reality, only the lattice ensembles with small pion mass have a good signal. From Fig. 9, we found that, for the (0.097, 0.0484) and (0.01, 0.05) ensembles, the plateaus are not too obvious, so in this work, we do not include these results.

Nevertheless, one thing greatly comforting us is that the interaction between two pions in this channel is not too weak, such that the discrete energies in a torus are shifted relatively bigger than those of the $I = 2$ channel from the values relevant for noninteracting pions, and as we can see from Tables II and VII, the energy shift between the interacting and noninteracting $\pi\pi$ states is not too small a fraction of total energy. This indicates that the rigorous calculation of disconnected diagrams is at present the most important thing.

The center-of-mass scattering momentum k^2 is calculated by Eq. (5) with pion masses listed in Table II, and then the corresponding s-wave scattering lengths $m_\pi a_{\pi\pi}^{I=0}$ can be obtained through Eq. (6). All of these values are summarized in Table VII, where the statistical errors of k^2 are calculated from the statistical errors of the energies aE and pion mass am_π, and its systematic errors are only estimated from the systematic errors of aE. Likewise, the statistical errors for $m_\pi a_{\pi\pi}^{I=0}$ are computed from the statistical errors of k^2 and am_π, and its systematic errors are estimated from the systematic errors of k^2 and one finite volume effect [27].

As already explained in the previous section, the dependence on the effective range r is small, and the range truncation actually leads to the finite volume correction at $O(L^{-6})$ in Lüscher formula (6) [26]. In practice, we compute this correction for each lattice ensemble, as suggested in Ref. [26]. These finite volume corrections have been combined in quadrature to the systematical errors listed in Table VII. Other sources of systematic uncertainty such as nonuniversal exponentially suppressed corrections [83], pion mass corrections [26,31,83], etc. are believed to be very small as compared with the rather large systematic error of the energies aE, or we currently do not have enough computational resources to fulfill them. With more

TABLE VII. Summaries of the lattice results for the fitted energies of the $\pi\pi$ system for the $I = 0$ channel. The second column shows the energies in lattice units, where the first uncertainties are statistical, and the second ones are the estimates of the systematic uncertainties. Column 3 shows the fitting range, and column 4 shows the number of degrees of freedom (d.o.f.) for the fit. The sixth column shows the center-of-mass scattering momentum k^2 in GeV, and column 7 gives the product of pion mass and scattering length, $m_\pi a_{\pi\pi}^{I=0}$, where the first uncertainty is statistical and the second one is systematic.

Ensemble	aE	Range	χ^2/d.o.f.	k^2 [GeV^2]	$m_\pi a_{\pi\pi}^{I=0}$
(0.00484, 0.0484)	0.33226(63)(78)	9–24	13.3/12	−0.00572(21)(24)	0.476(25)(29)
(0.005, 0.05)	0.3013(16)(18)	11–24	14.6/10	−0.00791(71)(76)	0.811(123)(133)
(0.007, 0.05)	0.3499(23)(26)	9–32	28.3/20	−0.0140(12)(13)	1.181(202)(223)

reliable calculation of the energies aE of the $\pi\pi$ system in the $I = 0$ channel in the future, these effects should eventually be incorporated into the more sophisticated lattice computation.

We should point out that, in this work, we do not quote our results for the (0.01, 0.05), (0.097, 0.0484) and (0.0194, 0.0484) ensembles due to two considerations: First, the vacuum contributions of these ensembles are noisy (see Fig. 3), and it is fairly difficult to see the clear plateau (see Fig. 9) in the effective energy plots. Second, the presence of the σ resonance is clearly presented in low energy [53,84], and thus it should be necessary for us to map out "avoided level crossings" between σ resonances and $\pi\pi$ states with isospin-0 to secure the reliable scattering length, as investigated in πK scattering in Refs. [53,84]. Luckily, as studied in Refs. [10,53,84], the contaminations from σ mesons for three lattice ensembles with small pion masses are negligible. Therefore, we only consider these results in the rest of the analysis.

VI. CHIRAL EXTRAPOLATIONS

In this work, we employed the rather small pion masses ranging from 240 to 463 MeV, which are still larger than the physical one. Therefore, χPT is needed to carry out a chiral extrapolation of the scattering lengths to the physical pion mass. The resulting NLO χPT formulas, which can be directly built from the results in Ref. [2] (see the Appendix for details), are described as [27,33]

$$m_\pi a_{\pi\pi}^{I=0} = \frac{7m_\pi^2}{16\pi f_\pi^2}\left\{1 - \frac{m_\pi^2}{16\pi^2 f_\pi^2}\left[9\ln\frac{m_\pi^2}{f_\pi^2} - 5 - l_{\pi\pi}^{I=0}(\mu = f_{\pi,\mathrm{phy}})\right]\right\}, \tag{20}$$

$$m_\pi a_{\pi\pi}^{I=2} = -\frac{m_\pi^2}{8\pi f_\pi^2}\left\{1 + \frac{m_\pi^2}{16\pi^2 f_\pi^2}\left[3\ln\frac{m_\pi^2}{f_\pi^2} - 1 - l_{\pi\pi}^{I=2}(\mu = f_{\pi,\mathrm{phy}})\right]\right\}, \tag{21}$$

where the values of m_π and f_π listed in Table II are inserted, and the χPT renormalization scale is fixed at the physical pion decay constant $\mu = f_{\pi,\mathrm{phy}}$. Wherever a quantity appears with a "phys" subscript, it refers to the value of that quantity in the physical case. The $l_{\pi\pi}^{I=0}(\mu)$ and $l_{\pi\pi}^{I=2}(\mu)$ are the combinations of the LECs in χPT at a quark-mass independent scale μ [25–27]. From the discussions in the Appendix, the $l_{\pi\pi}^{I=0}(\mu)$ and $l_{\pi\pi}^{I=2}(\mu)$ are connected to the LECs $\bar{l}_n$ as [2,85]

$$l_{\pi\pi}^{I=0} = \frac{40}{21}\bar{l}_1 + \frac{80}{21}\bar{l}_2 - \frac{5}{7}\bar{l}_3 + 4\bar{l}_4 + 9\ln\frac{m_\pi^2}{f_{\pi,\mathrm{phy}}^2}, \tag{22}$$

$$l_{\pi\pi}^{I=2} = \frac{8}{3}\bar{l}_1 + \frac{16}{3}\bar{l}_2 - \bar{l}_3 - 4\bar{l}_4 + 3\ln\frac{m_\pi^2}{f_{\pi,\mathrm{phy}}^2}. \tag{23}$$

It should be noted that Eqs. (20) and (21) are expressed in terms of the full f_π computed on the lattice, and not the physical value $f_{\pi,\mathrm{phy}}$. In reality, in the chiral expansion, the difference between utilizing f_π and $f_{\pi,\mathrm{phy}}$ in the argument of the logarithm only alters scattering lengths at higher orders [25,26].

As recommended in Refs. [25–27], we will carry out the extrapolation of the products $m_\pi a_{\pi\pi}^{I=2}$ and $m_\pi a_{\pi\pi}^{I=0}$ by means of the ratio m_π/f_π in place of m_π. From the Appendix, we note that extrapolating in m_π/f_π in lieu of m_π does transform the representations for $m_\pi a_{\pi\pi}^{I=2}$ and $m_\pi a_{\pi\pi}^{I=0}$ but only at NNLO or higher. Additionally, since m_π/f_π is a dimensionless quantity, there is no systematic error arising from the scale setting [25–27].

We should remark that the lattice calculations reported here used two lattice spacings of 0.15 fm and 0.12 fm. Thus, it is meaningless to directly compare the energies aE of the $\pi\pi$ system. However, on the assumption that the Lüscher technique properly explains the finite volume dependence of the energies aE for these lattice ensembles, we can compare $m_\pi a_{\pi\pi}^{I=2}$ and $m_\pi a_{\pi\pi}^{I=0}$ for two lattice spacings [27], and we observe such agreement with statistical error in Table V.

A. $I = 2$ channel

We are now in a position to fit lattice results of $m_\pi a_{\pi\pi}^{I=2}$ in Table V to the NLO χPT functional form (21) to obtain the low-energy constant $l_{\pi\pi}^{I=2}(\mu = f_{\pi,\mathrm{phy}})$, and then the extrapolated value at the physical point $(m_\pi a_{\pi\pi}^{I=2})_{\mathrm{phys}}$ can be obtained. The lattice-calculated values of $m_\pi a_{\pi\pi}^{I=2}$ as the function of m_π/f_π are shown in Fig. 10, and the outer error on the extrapolated result represents the systematic error

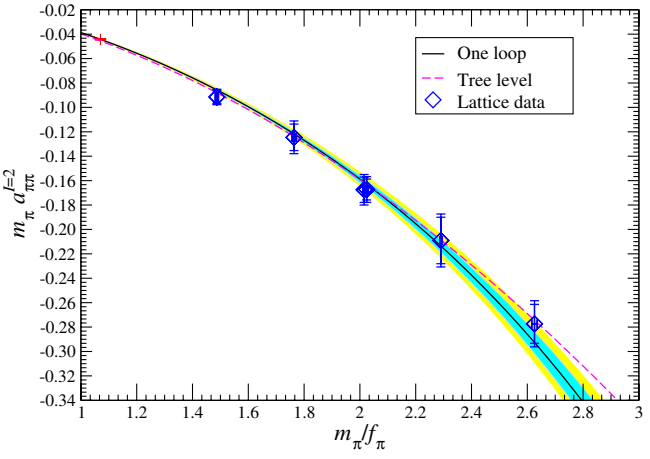

FIG. 10 (color online). The lattice-measured values of $m_\pi a_{\pi\pi}^{I=2}$ as a function of m_π/f_π. The red plus point indicates the scattering length at the physical limit, $(m_\pi a_{\pi\pi}^{I=2})_{\mathrm{phys}}$. The shaded bands correspond to statistical (inner, cyan) errors and statistical and systematic errors combined in quadrature (outer, yellow). The solid (black) curve is the central value of the NLO χPT fit. The dashed (magenta) line is the tree-level χPT prediction.

and statistical error combined in quadrature. The one-loop χPT fit curve is displayed by the black solid line, and the red plus point indicates its physical s-wave scattering length, $(m_\pi a_{\pi\pi}^{I=2})_{\rm phys}$, which is the chiral extrapolation of $m_\pi a_{\pi\pi}^{I=2}$ at the physical limit. In the same figure, we present the tree-level prediction as well. It is important to note that lattice data manifest fairly small displacement from the tree-level forecast. Additionally, we notice that our lattice results for $m_\pi a_{\pi\pi}^{I=2}$ are in general agreement with the one-loop formula. In fact, the deviation of $(m_\pi a_{\pi\pi}^{I=2})_{\rm phys}$ from the tree-level prediction is a natural aftermath of NLO χPT fitting [27].

In principle, we can fit our lattice-calculated data to the NNLO χPT form for $m_\pi a_{\pi\pi}^{I=2}$ [2,3] [see the concrete form in Eq. (A10)], as in Ref. [31], since we have six lattice data at our disposal. In the meantime, we can make an estimate of NNLO LECs with a careful analysis for the chiral extrapolation of $m_\pi a_{\pi\pi}^{I=2}$, since we have lattice data points at the lighter quark masses. However, the NNLO fit has larger errors in both $l_{\pi\pi}^{I=2}$ and $m_\pi a_{\pi\pi}^{I=2}$ than those with NLO fit, as shown in Refs. [25–27,31], and the errors of the LECs $l_{\pi\pi,I=2}^{(2)}$ and $l_{\pi\pi,I=2}^{(3)}$ are rather large, like the corresponding obtained values in Ref. [31]. Therefore, the calculations of NNLO LECs with physical meaning cannot be obtained in this work. A rigorous NNLO χPT fit should wait for more lattice data at pion masses closer to the physical point than we presently have. Admittedly, the resulting NNLO extrapolated value of $m_\pi a_{\pi\pi}^{I=2}$ is indeed in harmony with NLO fit, as we expect [27]. Actually, we use the NNLO χPT functional form to estimate systematic errors due to truncating the χPT series to NLO form [25].

As practiced in Ref. [27], we only consider three major sources of systematic uncertainty on the extrapolated value of $m_\pi a_{\pi\pi}^{I=2}$ and $l_{\pi\pi}^{I=2}$. First, the lattice-calculated systematic errors of $m_\pi a_{\pi\pi}^{I=2}$ per ensemble are spread by the chiral extrapolation [27]. Second, the systematic error inherently stems from the NLO χPT fit [25,26], which can be roughly calculated by taking the discrepancy between the NLO χPT extrapolated value from all six data sets and that from "pruning" the heaviest data set [27]. Third, the experimental errors on m_π and f_π [86] give rise to another important source of systematic error [27]. All three components are combined in quadrature to make up the entire systematic error. Taking the latest PDG data [86] for the most accurate charged pion mass $m_\pi = m_{\pi^+} = 139.57018(35)$ MeV and pion decay constant $f_\pi = f_{\pi^+} = 130.41(20)$ MeV, where a couple of experimental errors are added in quadrature, and hence $m_\pi/f_\pi = 1.07024(166)$, we finally secure the upshots

$$\begin{aligned} m_\pi a_{\pi\pi}^{I=2} &= -0.04430(25)(40), \\ l_{\pi\pi}^{I=2}(\mu = f_{\pi,\rm phys}) &= 3.27(.77)(1.12), \end{aligned} \tag{24}$$

where the first uncertainty is statistical and the second one is an estimate of the systematic error.

These outcomes are comparable with the aforementioned results of theoretical (or phenomenological) studies [1,3,7,9,10], experimental determinations [11,15,16], and lattice calculations [25–27,31] within statistical errors. The relevant results for $m_\pi a_{\pi\pi}^{I=2}$ are courteously compiled in Table VIII. The first group is lattice QCD results. The second one is theoretical (or phenomenological)

TABLE VIII. A compilation of the various theoretical (or phenomenological), experimental, and lattice QCD determinations of $m_\pi a_{\pi\pi}^{I=2}$ extracted from the literature. Together with every reference, for an easier comparison, the first author name or the collaborations are given. The first uncertainty is statistical and second one is systematic if provided.

References	$m_\pi a_{\pi\pi}^{I=2}$	Remarks
This work	$-0.04430 \pm 0.00025 \pm 0.00040$	The calculation made in this paper
Yagi [31]	$-0.04410 \pm 0.00069 \pm 0.00018$	Extrapolation with NNLOχPT
Xu [27]	$-0.04385 \pm 0.00028 \pm 0.00038$	Using two flavors of maximally twisted mass fermions
NPLQCD [26]	-0.04330 ± 0.00042	Error combines statistical and systematic errors in quadrature
CLQCD [20]	-0.0399 ± 0.0070	The result from Scheme I of anisotropic lattices
NPLQCD [25]	$-0.0426 \pm 0.0006 \pm 0.0003$	With fully dynamical domain-wall valence-quark propagators
Du [23]	-0.0467 ± 0.0045	Using anisotropic lattices in an asymmetric box
CP-PACS [24]	-0.0413 ± 0.0029	Compensating the mass dependence of the scattering length
JLQCD [22]	-0.0410 ± 0.0069	Selecting the result from EXP, which employs a single exponential
Albaladejo [10]	-0.0424 ± 0.0012	Employing unitary chiral perturbation theory
Guo [9]	-0.0444 ± 0.0011	Providing full results for all the contributing $\mathcal{O}(p^6)$ couplings
Sasaki [8]	-0.0431 ± 0.0015	Obtaining directly from the $\pi\pi$ wave function
MILC [68]	-0.0433 ± 0.0009	Using MILC's determinations of LECs along with Roy equations
Zhou [7]	-0.0440 ± 0.0011	Chiral unitarization with crossing symmetry and phase shift data
CGL [3]	-0.0444 ± 0.0010	Two-loop accuracy
Weinberg [1]	-0.04557 ± 0.00014	Tree-level prediction
NA48/2 [15,16]	$-0.0429 \pm 0.0044 \pm 0.0016$	With independent experimental errors and different theoretical inputs
E865 [11]	$-0.0454 \pm 0.0031 \pm 0.0010$	With the χPT constraints in the analysis

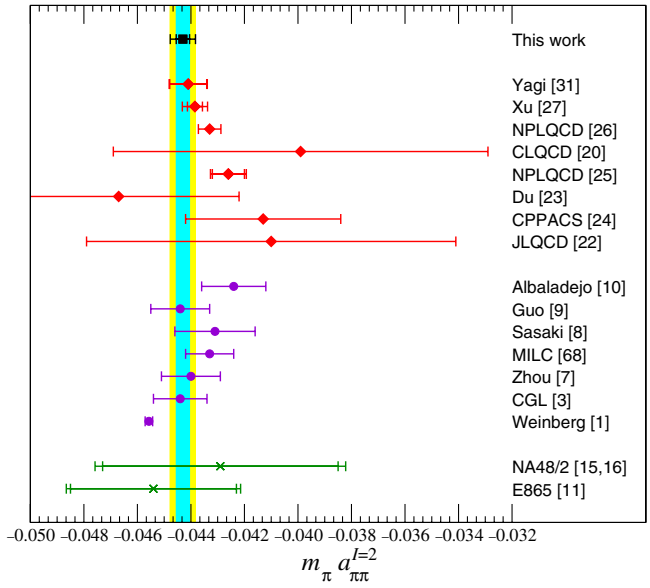

FIG. 11 (color online). A collection of the various lattice QCD, theoretical (or phenomenological), and experimental results of $m_\pi a_{\pi\pi}^{I=2}$ listed in Table VIII. The lattice studies are shown by red diamonds, purple circles are theoretical (or phenomenological) predictions, and the experimental ones are given by green crosses. Our result is indicated by a black square. For an easier comparison, the (cyan) inner strip corresponds to the statistical error whereas the (yellow) outer strip represents the statistical and systematic errors added in quadrature.

studies. Also included are two experimental values in the third group.

To make our demonstrations of these results more intuitive, they are offered graphically in Fig. 11, where we clearly note that the various results for every $m_\pi a_{\pi\pi}^{I=2}$ are fairly compatible with one another within errors.

Our calculation of the LEC $l_{\pi\pi}^{I=2}$ is satisfactory as well. Although it only has around 25% precision, it is comparable with relevant results obtained by phenomenological predictions [3], experimental determinations [11,15,16], and lattice calculations [25–27,31]. The relevant values of $l_{\pi\pi}^{I=2}$ are collected in Table IX. The first group is lattice results. The second one is phenomenological and experimental determinations, which are transformed directly from the experimental and phenomenological results of $m_\pi a_{\pi\pi}^{I=2}$ into $l_{\pi\pi}^{I=2}$ at NLO χPT, as preformed in Ref. [27].

The reason why we made a significant improvement in precision over our previous work [33] is the recent comprehension of various lattice-spacing artifacts (in particular, the wraparound effect). In fact, the approximate 0.5% accuracy of our ultimate result for $m_\pi a_{\pi\pi}^{I=2}$ is typically a joint effort from lattice QCD and χPT. This can be understood from two aspects: First, we have lattice data closer to the physical point, which have relatively smaller uncertainties for $m_\pi a_{\pi\pi}^{I=2}$. Second, the chiral extrapolation of $m_\pi a_{\pi\pi}^{I=2}$ is considerably restricted by χPT and $m_\pi a_{\pi\pi}^{I=2}$ is solely predicted in terms of m_π/f_π at LO and depends

TABLE IX. Some values of $l_{\pi\pi}^{I=2}$ extracted from the literature. The first uncertainty is statistical, and the second one is systematic if present. The first group is lattice QCD results. The second one is phenomenological and experimental determinations, which are transformed directly from the corresponding results of $m_\pi a_{\pi\pi}^{I=2}$ into $l_{\pi\pi}^{I=2}$ at NLO χPT [27].

References	$l_{\pi\pi}^{I=2}$
This work	$3.27 \pm 0.77 \pm 1.12$
Yagi [31]	5.8 ± 1.2
Xu [27]	$4.65 \pm 0.85 \pm 1.07$
NPLQCD [26]	6.2 ± 1.2
NPLQCD [25]	$3.3 \pm 0.6 \pm 0.3$
CGL [3]	3.0 ± 3.1[a]
NA48/2 [15,16]	$7.5 \pm 13.3 \pm 4.8$[b]
E865 [11]	$0.0 \pm 9.4 \pm 3.0$

[a]It is interesting to note that if we make use of Eq. (23) with the values of $\bar{l}_i$ reported in Ref. [3], and necessary PDG values, we obtain $l_{\pi\pi}^{I=2} = 2.0 \pm 3.1$.
[b]Using the data from Ref. [15].

uniquely upon a LEC, $l_{\pi\pi}^{I=2}$, at NLO. This means that the statistical error of NLO χPT extrapolation of $m_\pi a_{\pi\pi}^{I=2}$ solely rests on the statistical error of $l_{\pi\pi}^{I=2}$. Consequently, although our lattice-calculated results of $m_\pi a_{\pi\pi}^{I=2}$ are only within about 6%–10% accuracy, we still obtain a less than 1% precise determination of $(m_\pi a_{\pi\pi}^{I=2})_{\rm phys}$.

B. $I = 0$ channel

We are now in a position to fit the lattice results of $m_\pi a_{\pi\pi}^{I=0}$ in Table VII to NLO χPT functional form (20) to secure the low-energy constant $l_{\pi\pi}^{I=0}(\mu = f_{\pi,\rm phy})$, and then we can obtain the extrapolated value at the physical point $(m_\pi a_{\pi\pi}^{I=0})_{\rm phys}$. The lattice-measured values of $m_\pi a_{\pi\pi}^{I=0}$ as the function of m_π/f_π are demonstrated in Fig. 12. The one-loop χPT fit curve is displayed by the solid black line, and the red circle point indicates its physical s-wave scattering length, $(m_\pi a_{\pi\pi}^{I=0})_{\rm phys}$, which is the chiral extrapolation of the $m_\pi a_{\pi\pi}^{I=0}$ at the physical point. In the same figure, we present the tree-level prediction as well. It is important to note that lattice data manifest a rather large displacement from the tree-level χPT forecast, which is consistent with a conclusion of Ref. [3] that the NLO corrections make about a 25% modification to the tree-level prediction. Additionally, we can notice that our lattice results for $m_\pi a_{\pi\pi}^{I=0}$ generally agree with the one-loop formula. The large deviation of $(m_\pi a_{\pi\pi}^{I=0})_{\rm phys}$ from the tree-level prediction is entirely a natural aftermath of the NLO χPT fitting.

In this work we cannot fit our lattice-calculated data to the NNLO χPT functional form (20) [2,3] [see concrete form (A10)], since we only have three lattice data at our disposal. A NNLO χPT determination should wait for more lattice data at pion masses closer to the physical point than we now have. Admittedly, as explained in detail in

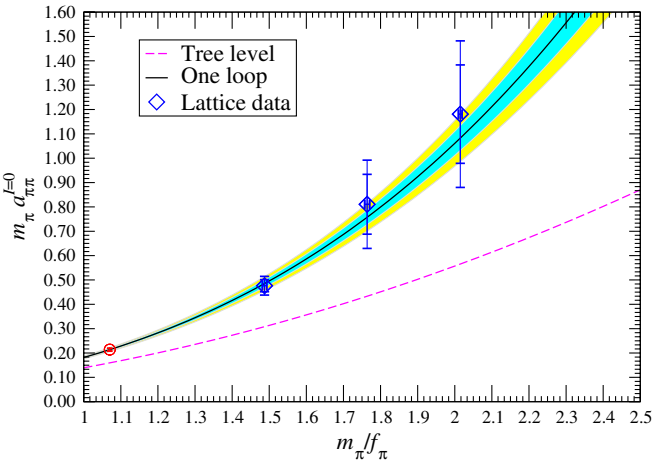

FIG. 12 (color online). The lattice-measured values of $m_\pi a_{\pi\pi}^{I=0}$ as a function of m_π/f_π. The red circle point indicates the scattering length at the physical limit, $(m_\pi a_{\pi\pi}^{I=0})_{\rm phys}$. The shaded bands correspond to statistical (inner, cyan) errors and statistical and systematic errors combined in quadrature (outer, yellow). The solid (black) curve is the central value of the NLO χPT fit. The dashed (magenta) line is the tree-level χPT prediction.

Ref. [3], the NLO correction increases the LO prediction by about 25%, and the NNLO correction further raises the LO prediction by more than 10%; this means that the NNLO χPT determination of $m_\pi a_{\pi\pi}^{I=0}$ should be significantly more rigorous than the NLO χPT determination of $(m_\pi a_{\pi\pi}^{I=0})_{\rm phys}$, and this can in part explain the relatively large error for our final NLO χPT extrapolated result of $(m_\pi a_{\pi\pi}^{I=0})_{\rm phys}$. As a consequence, the systematic error from truncating the χPT series to the NLO form should be considered.

In this work, we only consider two major sources of systematic errors in the extrapolated value of $m_\pi a_{\pi\pi}^{I=0}$, since the systematic error from the experimental errors on m_π and f_π is found to be fairly small as compared with its statistical error. First, the lattice-computed systematic errors of $m_\pi a_{\pi\pi}^{I=0}$ per ensemble are propagated via the chiral extrapolation. Second, the systematic error inherently stems from the NLO fit, which is computed by taking the difference between the extrapolated values from the NLO fit to all three data sets and then from "cropping" the heaviest data set [27]. Both parts are added in quadrature to give the whole computed systematic error. We get the final upshot

$$\begin{aligned} m_\pi a_{\pi\pi}^{I=0} &= 0.214(4)(7), \\ l_{\pi\pi}^{I=0}(\mu = f_{\pi,\rm phys}) &= 43.2 \pm 3.5 \pm 5.6, \end{aligned} \tag{25}$$

where the numbers in the first and second parentheses are the statistical and systematic uncertainties, respectively.

These results can be fairly comparable with the above-mentioned results by theoretical (or phenomenological) studies [1,3,7,9,10,87,88] (except the tree-level prediction) and experimental determinations [11,15,16]. The relevant results for $m_\pi a_{\pi\pi}^{I=0}$ are compiled in Table X. The first group is lattice results. The second one is theoretical (or phenomenological) studies. Two experimental values are also given in the third group.

To make our report of these results more intuitive, these results are given graphically in Fig. 13 as well, where the various results of $m_\pi a_{\pi\pi}^{I=0}$ are compatible with one another within errors, except for the tree-level prediction [1] and our crude lattice study [33].

Our calculation of the LEC $l_{\pi\pi}^{I=0}$ is satisfactory as well. Although it is within about 5% accuracy, nevertheless, as we show soon, this result can be comparable with the results of phenomenological [3] and experimental determinations [11,15,16] and lattice studies [25–27,31]. The relevant values of $l_{\pi\pi}^{I=0}$ are collected in Table XI. The first group is lattice results. The second one is phenomenological and experimental determinations, which are converted directly from the experimental phenomenological results of $m_\pi a_{\pi\pi}^{I=0}$ into $l_{\pi\pi}^{I=0}$ at NLO χPT as conducted by Xu *et al.* in Ref. [27] for the $I = 2$ channel.

TABLE X. A compilation of the various theoretical (or phenomenological), experimental, and lattice QCD determinations of $m_\pi a_{\pi\pi}^{I=0}$ extracted from the literature. Together with every reference, for an easier comparison, the first author or the collaborations are given. The first uncertainty is statistical and the second one is systematic if given.

References	$m_\pi a_{\pi\pi}^{I=0}$	Remark
This work	$0.214 \pm 0.004 \pm 0.007$	Full QCD
Fu [33]	0.186 ± 0.002	Partially quenched QCD
Albaladejo [10]	0.219 ± 0.005	Employing unitary chiral perturbation theory
Guo [9]	0.220 ± 0.005	Full results for all the contributing $\mathcal{O}(p^6)$ couplings
Caprini [88]	0.218 ± 0.014	Using a large class of analytic parametrizations
Yndurain [87]	0.233 ± 0.013	Extrapolating to the pole of the sigma resonance
Zhou [7]	0.211 ± 0.011	Using chiral unitarization with crossing symmetry and phase shift data
CGL [3]	0.220 ± 0.005	Two-loop accuracy
Weinberg [1]	0.1595 ± 0.0005	Tree-level prediction
NA48/2 [15,16]	$0.2210 \pm 0.0047 \pm 0.0015$	With independent experimental errors and different theoretical inputs
E865 [11]	$0.216 \pm 0.013 \pm 0.002$	With the χPT constraints in the analysis

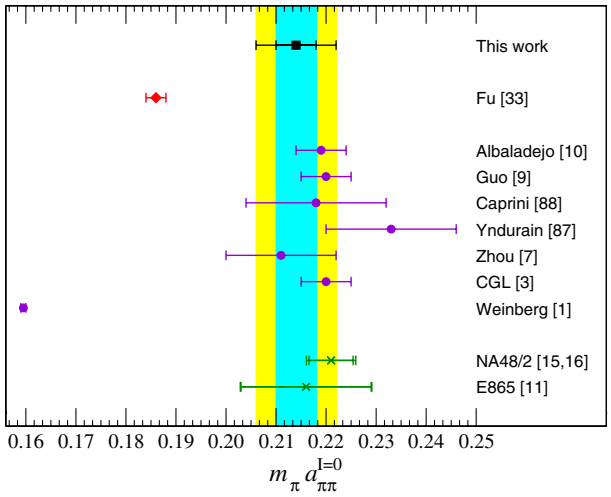

FIG. 13 (color online). A collection of various lattice QCD, theoretical (or phenomenological), and experimental results of $m_\pi a_{\pi\pi}^{I=0}$ listed in Table X. The red diamonds are lattice determinations, purple circles are theoretical (or phenomenological) studies, and experimental ones are represented by green crosses. Our result is shown by a black square. For an easier comparison, the (cyan) inner strip corresponds to the statistical error whereas the (yellow) outer strip represents the statistical and systematic errors added in quadrature.

The remarkable improvement in accuracy over our previous results [33] is a joint effort from lattice QCD and χPT. First, we have measured the lattice data closer to the physical point, which has smaller uncertainties. Second, chiral perturbation theory considerably constrains the chiral extrapolation of the product $m_\pi a_{\pi\pi}^{I=0}$, which is uniquely predicted in terms of m_π/f_π at LO and relies solely on a LEC, $l_{\pi\pi}^{I=0}$, at NLO. This suggests that the statistical error of NLO χPT extrapolation of $m_\pi a_{\pi\pi}^{I=0}$ solely rests on the statistical error of $l_{\pi\pi}^{I=0}$. Consequently, although our lattice-calculated results of $m_\pi a_{\pi\pi}^{I=0}$ are only within 5%–17% accuracy, we still obtain about a 2% precise determination of $(m_\pi a_{\pi\pi}^{I=0})_{\text{phys}}$.

TABLE XI. Some values of $l_{\pi\pi}^{I=0}$ extracted from the literature. The first uncertainty is statistical, and the second one is systematic if present. The first group is lattice simulation results. The second one is phenomenological and experimental determinations, which are directly transformed from the corresponding results of $m_\pi a_{\pi\pi}^{I=0}$ into $l_{\pi\pi}^{I=0}$ at NLO χPT [27].

	$l_{\pi\pi}^{I=0}$
This work	$43.2 \pm 3.5 \pm 5.6$
Fu [33]	18.7 ± 1.2
CGL [3]	48.5 ± 4.3[a]
NA48/2 [15]	$49.3 \pm 4.1 \pm 1.3$
E865 [11]	$45.0 \pm 11.2 \pm 3.5$

[a]If we make use of Eq. (22) with the values of $\bar{l}_i$ reported in Ref. [3], and required PDG values, we get $l_{\pi\pi}^{I=0} = 32.4 \pm 2.3$.

VII. SUMMARY AND OUTLOOK

We have reported results of a lattice QCD calculation of the s-wave $\pi\pi$ scattering lengths for both $I = 0$ and 2 channels on the MILC medium-coarse ($a \approx 0.15$ fm) and coarse ($a \approx 0.12$ fm) lattice ensembles with the $2 + 1$ flavors of the Asqtad-improved staggered sea quarks. We exploited the moving wall sources without the gauge fixing [18,19] to compute all four diagrams assorted in Refs. [17,18], and we viewed a clear attractive signal for the $I = 0$ channel and a good repulsive one for the $I = 2$ channel, respectively. Moveover, extrapolating our lattice data of the s-wave scattering lengths for both isospin eigenstates to the physical pion mass gives the scattering lengths $m_\pi a_{\pi\pi}^{I=2} = -0.04430(25)(40)$ and $m_\pi a_{\pi\pi}^{I=0} = 0.214(4)(7)$ for the $I = 2$ and 0 channels, respectively, which are in fair agreement with the current theoretical (or phenomenological) predictions to one-loop levels and the present experimental reports, and they can be comparable with other lattice studies.

After our extremely crude estimation of the $\pi\pi$ scattering length in the $I = 0$ channel in Ref. [33], and this relatively more sophisticated computation, we can fairly claim that even with limited computing resources, the lattice calculation of the $\pi\pi$ scattering length in the $I = 0$ channel is feasible, although this work absolutely needs to be further improved, and the various sources of systematic error need to be clarified thoroughly. Most of all, from this work, we found that the rule of thumb estimation of lattice ensemble with the Goldstone pion mass eligible to study s-wave $\pi\pi$ scattering in the $I = 0$ channel should be less than about 300 MeV (the smaller, the better), which is very helpful for researchers to pursue this fascinating enterprise. We view it as one of the important results of this work.

As we revealed, a reasonable signal can be gained for the (0.00484, 0.0484) and (0.005, 0.05) ensembles in the vacuum diagram of $\pi\pi$ scattering. In principle, the signal-to-noise ratio can be further enhanced by launching the same calculation on the lattice ensembles with a smaller pion mass (of course, we can also improve the statistics by using more lattice gauge configurations or performing the calculation on a larger volume). In addition, the behavior close to the physical point is intensely influenced by the chiral logarithm term, so an extraction of the $\pi\pi$ scattering lengths without a long extrapolation is still much needed to guarantee the convergence of the chiral expansion. Fortunately, the MILC collaboration has generated enough lattice ensembles whose Goldstone pion masses are smaller than or close to 240 MeV [89,90] [e.g., the fine (0.00155, 0.0310) ensemble, whose Goldstone pion mass is about 177 MeV]. Furthermore, as we explained early, the NNLO χPT will be the proper physical functional form to fit the lattice data (at least four data points) of the $I = 0$ $\pi\pi$ scattering length and it needs more lattice data near the physical point. We have an impetus to do these works. However, it is beyond the

scope of this work, since this will need an astronomical amount of computing allocations. We will enthusiastically appeal for all the possible computational resources to accomplish this peculiar and challenging task.

It is well known that $\pi\pi$ scattering in the $I = 0$ channel is challenging and stimulating phenomenologically due to the existence of the σ resonance. In this work, we have exhibited that $\pi\pi$ scattering for the $I = 0$ channel can be reliably calculated by the moving wall sources without gauge fixing [18,19]. It prompts us to anticipate that this technique can be successfully exploited to study the σ resonance. In our previous work [77], we evaluated the σ mass from lattice QCD and found that the decay $\sigma \to \pi\pi$ is allowed kinematically only for a small enough u quark mass. This work and our lattice calculation for the $\pi\pi$ scattering lengths delivered in this paper will encourage researchers to study the σ resonance. We have been investigating the σ resonance parameters with the isospin representation of $(I, I_z) = (0, 0)$, and the preliminary lattice results are already reported in Ref. [54].

Additionally, for $\pi\pi$ scattering in the $I = 0$ channel, we realize an important issue: the presence of σ resonance is possible at low energy, and thus it should be necessary for us to employ the variational method [38] to secure the rigorous scattering length, as investigated in πK scattering in the $I = 1/2$ channel in Refs. [53,84]. Since we only make use of relatively small quark masses to study $\pi\pi$ scattering in the $I = 0$ channel, we can temporarily and reasonably overlook this contamination in the present study, as already explained in Ref. [53]. However, we should bear in mind that this issue should be settled in the more sophisticated lattice examination. It will be very interesting to systematically study this pollution for $\pi\pi$ scattering in the $I = 0$ channel.

Admittedly, due to the intense theoretical and experimental efforts recently put into the scalar-isoscalar and scalar-isovector sector of meson-meson scattering, studying the $K\bar{K}$ scattering length on the lattice is gradually becoming a very interesting enterprise. As pointed out in Ref. [91], the robust calculation of the $\pi\pi$ scattering lengths (in particular for the $I = 0$ channel) will naturally encourage us to study other challenging systems like $K\bar{K}$, etc. Physically, as explained in Refs. [60,65,92], studying $K\bar{K}$ is very important, and the calculation of the s-wave $K\bar{K}$ scattering length in the $I = 0$ channel is a genuine two-coupled-channel problem [65,93], where the system can be approximately described only by two $\pi\pi$ and $K\bar{K}$ channels (we refer to $\pi\pi$ as channel 1 and $K\bar{K}$ channel 2); then the S matrix is a 2×2 unitary matrix which contains three real parameters [65,93] (the s-wave $K\bar{K}$ scattering in the $I = 1$ channel can be treated analogously [59], and the lattice study of $\pi\eta$ scattering is then highly desirable). Therefore, it is absolutely necessary to incorporate the s-wave $I = 0$, $\pi\pi$ channel for a physical calculation of the s-wave $K\bar{K}$ scattering length in the $I = 0$ channel. The generalized Lüscher's formula in this case gives a relation among these three parameters, all of which are functions of the energy [93]. Since some of these parameters are still poorly measured in the present experiments, the lattice calculation is valuable and highly desirable. With our lattice efforts on channel 2 in Ref. [60], at present, if we can compute s-wave $\pi\pi \to K\bar{K}$ scattering in the $I = 0$ channel, in principle, we can solve this problem. We are launching a series of lattice studies toward these aims.

ACKNOWLEDGMENTS

We feel much indebted to the MILC Collaboration for using the Asqtad lattice ensembles and MILC codes. We should thank NERSC for providing us the platform to download MILC gauge configurations, and Dr. Massimo Di Pierro for his wonderful Python toolkit. The author profoundly thanks Carleton DeTar for indoctrinating me in the necessary theoretical knowledge and computational skills for this work during my Ph.D. study at the University of Utah, and supplying me with the required software. The author deeply appreciates Paul Kienzle for teaching me computer skills during my work in NIST, Gaithersburg, USA. The author heartily thanks the Grace Development Team for the use of xmgrace. We especially thank Eulogio Oset for his enlightening and constructive comments and corrections. The author must express my respect to Sasa Prelovsek and Liu Chuan for reading this manuscript and giving some valuable comments. The author would like to express his gratitude to the Institute of Nuclear Science and Technology, Sichuan University, where the computer resources and technical support are provided (in particular Hou Qing, [94] Zhu An, Ning Liu, and Jun Wang). Numerical calculations for this paper were carried out at AMAX, CENTOS, and HP workstations. Parts of numerical calculations were conducted at the Utah Center for High Performance Computing, University of Utah, during my Ph.D. study.

APPENDIX: SCATTERING LENGTH OF $\pi\pi$ IN χPT AT NNLO

In Ref. [33], we provided the compact continuum three-flavor χPT form for the s-wave $\pi\pi$ scattering length for isospin-0 at the NLO in the continuum limit of QCD by constructing from Appendix C in Ref. [2]. Here we follow the original derivations and notations in Refs. [2–4,31] to derive its compact form at the NNLO.

The $\pi\pi$ scattering lengths are provided at the NNLO of χPT in Refs. [2–4], and the s-wave $\pi\pi$ scattering length in the $I = 0$ channel is described as [2–4]

$$m_\pi a_{\pi\pi}^{I=0} = \frac{7m_\pi^2}{32\pi f_\pi^2}\Big\{1 + \frac{x}{7}[49 + 5\bar{b}_1 + 12\bar{b}_2 + 48\bar{b}_3 + 32\bar{b}_4] + x^2\Big[\frac{7045}{63} - \frac{215\pi^2}{126} + 10\bar{b}_1 + 24\bar{b}_2 + 96\bar{b}_3 + 64\bar{b}_4 + \frac{192}{7}\bar{b}_5\Big]\Big\} + \mathcal{O}(x^4), \quad \text{(A1)}$$

where $x = m_\pi^2/(16\pi^2 f_\pi^2)$ is the chiral expansion parameter and $\bar{b}_i$'s are dimensionless combinations of the coupling constants introduced in Refs. [2,3] to parametrize the pion scattering amplitude. After some strenuous algebraic manipulations, we can check that

$$5\bar{b}_1 + 12\bar{b}_2 + 48\bar{b}_3 + 32\bar{b}_4 = \frac{63}{2}\tilde{L} - \frac{503}{6}x\tilde{L}^2 - \frac{20}{3}\tilde{l}_1 + \frac{40}{3}\tilde{l}_2 - \frac{5}{2}\tilde{l}_3 + 14\tilde{l}_4 - \frac{63}{2} + x\tilde{L}\left(-\frac{388}{3}\tilde{l}_1 - \frac{472}{3}\tilde{l}_2 - 35\tilde{l}_3 + 154\tilde{l}_4 + \frac{1405}{12}\right) + x\left(\frac{80}{3}\tilde{l}_1\tilde{l}_4 + \frac{160}{3}\tilde{l}_2\tilde{l}_4 - 15\tilde{l}_3\tilde{l}_4 + 35\tilde{l}_4^2 - \frac{5}{2}\tilde{l}_3^2 + \frac{364}{3}\tilde{l}_1 + \frac{1336}{9}\tilde{l}_2 + \frac{141}{4}\tilde{l}_3 - 126\tilde{l}_4 + \frac{162719}{432} - \frac{373}{18}\pi^2 + 5\tilde{r}_1 + 12\tilde{r}_2 + 48\tilde{r}_3 + 32\tilde{r}_4\right), \quad \text{(A2)}$$

where the low-energy constants $\tilde{l}_i$, $\tilde{r}_i$ are the quark-mass independent couplings from the subleading orders $\mathcal{L}_4$, $\mathcal{L}_6$ of the effective Lagrangian, respectively [3], and renormalized at the running scale μ; and $\tilde{L} = \ln(\mu^2/m_\pi^2)$.

Inserting Eq. (A2) into Eq. (A1) and considering expression B.3 of Ref. [3],

$$\bar{b}_5 = \frac{85}{72}\tilde{L}^2 + \tilde{L}\left\{\frac{7}{8}\tilde{l}_1 + \frac{107}{72}\tilde{l}_2 - \frac{625}{288}\right\} + \tilde{r}_5 + \frac{7}{54}\pi^2 - \frac{66029}{20736} + \mathcal{O}(x^4).$$

We recast the result in the order of x as

$$m_\pi a_{\pi\pi}^{I=0} = \frac{7m_\pi^2}{32\pi f_\pi^2}\left\{1 + \frac{x}{2}(9\tilde{L} + l_a^0) + x^2\left(\frac{857}{42}\tilde{L}^2 + l_b^0\tilde{L} + l_c^0\right)\right\} + \mathcal{O}(x^4), \quad \text{(A3)}$$

with

$$l_a^0 = \frac{40}{21}\tilde{l}_1 + \frac{80}{21}\tilde{l}_2 - \frac{5}{7}\tilde{l}_3 + 4\tilde{l}_4 + 5,$$
$$l_b^0 = \frac{116}{21}\tilde{l}_1 + \frac{128}{7}\tilde{l}_2 - 5\tilde{l}_3 - 22\tilde{l}_4 - \frac{3595}{84},$$
$$l_c^0 = \frac{5}{7}\tilde{r}_1 + \frac{12}{7}\tilde{r}_2 + \frac{48}{7}\tilde{r}_3 + \frac{32}{7}\tilde{r}_4 + \frac{192}{7}\tilde{r}_5 + \frac{80}{21}\tilde{l}_1\tilde{l}_4 + \frac{160}{21}\tilde{l}_2\tilde{l}_4 - \frac{15}{7}\tilde{l}_3\tilde{l}_4 + 5\tilde{l}_4^2 - \frac{5}{14}\tilde{l}_3^2 + \frac{148}{21}\tilde{l}_1 + \frac{232}{21}\tilde{l}_2 + \frac{1}{28}\tilde{l}_3 + 10\tilde{l}_4 - \frac{17561}{504} + \frac{394}{63}\pi^2. \quad \text{(A4)}$$

The right-hand side (rhs) of Eq. (A1) is scale independent [3]. On the whole, the rhs of Eq. (A3) is scale invariant as well. Therefore, in principle, we can select the running scale μ stochastically. However, when fitting our lattice-obtained scattering lengths as a function of x, it is highly desirable for us to set the fitting parameters to be quark-mass independent. As in Ref. [31], we select $\mu = 4\pi f_{\pi,\mathrm{phy}}$. Using this scale, we can see

$$\tilde{L}(\mu = 4\pi f_{\pi,\mathrm{phy}}) = -\ln x - 2x\tilde{l}_4(\mu = 4\pi f_{\pi,\mathrm{phy}}) + 2x\ln x + \mathcal{O}(x^2), \quad \text{(A5)}$$

where we exploit the chiral expansion of the pion decay constant $f_\pi = f_{\pi,\mathrm{phy}}\{1 + x\bar{l}_4 + \mathcal{O}(x^2)\}$ [3].

Plugging Eq. (A5) into Eq. (A3), and rearranging the result in the order of x, we achieve the $\pi\pi$ scattering length in the $I = 0$ channel as

$$m_\pi a_{\pi\pi}^{I=0} = \frac{7m_\pi^2}{32\pi f_\pi^2}\left\{1 + \frac{m_\pi^2}{32\pi^2 f_\pi^2}\left[-9\ln\left(\frac{m_\pi^2}{16\pi^2 f_\pi^2}\right) + l_a^0\right] + x^2\left[\frac{857}{42}(\ln x)^2 - (l_b^0 + 9)\ln x + (l_c^0 + 9\tilde{l}_4)\right]\right\} + \mathcal{O}(x^4). \quad \text{(A6)}$$

The continuum χPT forms for the s-wave $\pi\pi$ scattering length in the $I = 2$ channel $a_{\pi\pi}^{I=2}$ at the NNLO was presented by Yagi *et al.* in Ref. [31], namely,

$$m_\pi a_{\pi\pi}^{I=2} = -\frac{m_\pi^2}{16\pi f_\pi^2}\left\{1 + \frac{m_\pi^2}{32\pi^2 f_\pi^2}\left[3\ln\left(\frac{m_\pi^2}{16\pi^2 f_\pi^2}\right) + l_a^2\right] + x^2\left[-\frac{31}{6}(\ln x)^2 - (l_b^2 + 3)\ln x + (l_c^2 + 3\tilde{l}_4)\right]\right\} + \mathcal{O}(x^4), \quad \text{(A7)}$$

with

$$l_a^2 = -\frac{8}{3}\tilde{l}_1 - \frac{16}{3}\tilde{l}_2 + \tilde{l}_3 + 4\tilde{l}_4 - 1,$$
$$l_b^2 = -\frac{4}{3}\tilde{l}_1 - 8\tilde{l}_2 + \tilde{l}_3 - 2\tilde{l}_4 + \frac{119}{12},$$
$$l_c^2 = \frac{1}{2}\tilde{l}_3^2 - \left(\frac{16}{3}\tilde{l}_1 + \frac{32}{3}\tilde{l}_2 - 3\tilde{l}_3 - 5\tilde{l}_4\right)\tilde{l}_4 + \frac{4}{3}\tilde{l}_1 + \frac{16}{3}\tilde{l}_2 + \frac{7}{4}\tilde{l}_3 - 2\tilde{l}_4 + \frac{163}{16} - \frac{22}{9}\pi^2 - \tilde{r}_1 - 16\tilde{r}_4. \quad \text{(A8)}$$

In the above equations, f_π is the pion decay constant, which is originally written as F_π (around 92.4 MeV) [2–4]. In the present work, $\sqrt{2}F_\pi$ is denoted by f_π (about 130 MeV) for the convenience of fitting our lattice data. Then the above equations are recast as

$$m_\pi a_{\pi\pi}^{I=0} = \frac{7m_\pi^2}{16\pi f_\pi^2}\left\{1 - \frac{m_\pi^2}{16\pi^2 f_\pi^2}\left[9\ln\frac{m_\pi^2}{f_\pi^2} - 5 - l_{\pi\pi}^{I=0}\right] + \frac{m_\pi^4}{64\pi^2 f_\pi^4}\left[\frac{857}{42}\left(\ln\frac{m_\pi^2}{f_\pi^2}\right)^2 + l_{\pi\pi,I=0}^{(2)}\ln\frac{m_\pi^2}{f_\pi^2} + l_{\pi\pi,I=0}^{(3)}\right]\right\}, \quad \text{(A9)}$$

$$m_\pi a_{\pi\pi}^{I=2} = -\frac{m_\pi^2}{8\pi f_\pi^2}\left\{1 + \frac{m_\pi^2}{16\pi^2 f_\pi^2}\left[3\ln\frac{m_\pi^2}{f_\pi^2} - 1 - l_{\pi\pi}^{I=2}\right] + \frac{m_\pi^4}{64\pi^4 f_\pi^4}\left[-\frac{31}{6}\left(\ln\frac{m_\pi^2}{f_\pi^2}\right)^2 + l_{\pi\pi,I=2}^{(2)}\ln\frac{m_\pi^2}{f_\pi^2} + l_{\pi\pi,I=2}^{(3)}\right]\right\}, \quad \text{(A10)}$$

where $l_{\pi\pi}^{(i)}$s are the combinations of LECs in χPT at a quark-mass independent running scale, since all the LECs are independent of quark mass; therefore, we can regard them as the fitting parameters in the chiral extrapolation of the s-wave $\pi\pi$ scattering lengths [31].

From Eqs. (A4) and (A6)–(A8), we can easily get the specific forms of $l_{\pi\pi}^{I=0}$ and $l_{\pi\pi}^{I=2}$, which are related to the Gasser-Leutwyler coefficients $\bar{l}_i$ as [2,85]

$$l_{\pi\pi}^{I=0} = \frac{40}{21}\bar{l}_1 + \frac{80}{21}\bar{l}_2 - \frac{5}{7}\bar{l}_3 + 4\bar{l}_4 + 9\ln\frac{m_\pi^2}{f_{\pi,\mathrm{phy}}^2}, \quad \text{(A11)}$$

$$l_{\pi\pi}^{I=2} = \frac{8}{3}\bar{l}_1 + \frac{16}{3}\bar{l}_2 - \bar{l}_3 - 4\bar{l}_4 + 3\ln\frac{m_\pi^2}{f_{\pi,\mathrm{phy}}^2}, \quad \text{(A12)}$$

where we consider the equality $\bar{l}_n = \tilde{l}_n + \ln(m_\pi^2/\mu^2)$ [3].

These are the forms that we used in our previous work [33]. For the other $l_{\pi\pi}^{(i)}$'s, their explicit forms are given or can be inferred from Eqs. (A4) and (A6)–(A8). It is interesting and important to note that if we select the running scale $\mu = f_{\pi,\mathrm{phy}}$, we obtain the same expressions.

[1] S. Weinberg, Phys. Rev. Lett. **17**, 616 (1966).
[2] J. Bijnens, G. Colangelo, G. Ecker, J. Gasser, and M. E. Sainio, Nucl. Phys. **B508**, 263 (1997).
[3] G. Colangelo, J. Gasser, and H. Leutwyler, Nucl. Phys. **B603**, 125 (2001).
[4] G. Colangelo, J. Gasser, and H. Leutwyler, Phys. Lett. B **488**, 261 (2000).
[5] S. M. Roy, Phys. Lett. **36B**, 353 (1971).
[6] B. Ananthanarayan, G. Colangelo, J. Gasser, and H. Leutwyler, Phys. Rep. **353**, 207 (2001).
[7] Z. Y. Zhou, G. Y. Qin, P. Zhang, Z. Xiao, H. Q. Zheng, and N. Wu, J. High Energy Phys. 02 (2005) 043.
[8] K. Sasaki and N. Ishizuka, Phys. Rev. D **78**, 014511 (2008).
[9] Z. H. Guo and J. J. Sanz-Cillero, Phys. Rev. D **79**, 096006 (2009).
[10] M. Albaladejo and J. A. Oller, Phys. Rev. D **86**, 034003 (2012).
[11] S. Pislak, R. Appel, G. S. Atoyan, B. Bassalleck, D. R. Bergman, N. Cheung, S. Dhawan, H. Do *et al.*, Phys. Rev. D **67**, 072004 (2003).
[12] R. Garcia-Martin, R. Kaminski, J. R. Pelaez, J. R. de Elvira, and F. J. Yndurain, Phys. Rev. D **83**, 074004 (2011).
[13] J. R. Batley *et al.* (NA48/2 Collaboration), Eur. Phys. J. C **54**, 411 (2008).
[14] J. R. Batley *et al.* (NA48/2 Collaboration), Eur. Phys. J. C **70**, 635 (2010).
[15] A. Bizzeti, AIP Conf. Proc. **1374**, 639 (2011).
[16] R. Wanke, Nucl. Phys. B, Proc. Suppl. **210–211**, 193 (2011).
[17] S. R. Sharpe, R. Gupta, and G. W. Kilcup, Nucl. Phys. **B383**, 309 (1992).
[18] Y. Kuramashi, M. Fukugita, H. Mino, M. Okawa, and A. Ukawa, Phys. Rev. Lett. **71**, 2387 (1993).
[19] M. Fukugita, Y. Kuramashi, M. Okawa, H. Mino, and A. Ukawa, Phys. Rev. D **52**, 3003 (1995).
[20] X. Li *et al.* (CLQCD Collaboration), J. High Energy Phys. 06 (2007) 053.
[21] R. Gupta, A. Patel, and S. R. Sharpe, Phys. Rev. D **48**, 388 (1993).
[22] S. Aoki *et al.* (JLQCD Collaboration), Phys. Rev. D **66**, 077501 (2002).
[23] X. Du, G. W. Meng, C. Miao, and C. Liu, Int. J. Mod. Phys. A **19**, 5609 (2004).
[24] T. Yamazaki *et al.* (*CP*-PACS Collaboration), Phys. Rev. D **70**, 074513 (2004).
[25] S. R. Beane, P. R. Bedaque, K. Orginos, and M. J. Savage (NPLQCD Collaboration), Phys. Rev. D **73**, 054503 (2006).
[26] S. R. Beane, T. C. Luu, K. Orginos, A. Parreno, M. J. Savage, A. Torok, and A. Walker-Loud (NPLQCD Collaboration), Phys. Rev. D **77**, 014505 (2008).
[27] X. Feng, K. Jansen, and D. B. Renner, Phys. Lett. B **684**, 268 (2010).
[28] S. R. Beane, E. Chang, W. Detmold, H. W. Lin, T. C. Luu, K. Orginos, A. Parreño, M. J. Savage, A. Torok, and A. Walker-Loud (NPLQCD Collaboration), Phys. Rev. D **85**, 034505 (2012).
[29] J. J. Dudek, R. G. Edwards, M. J. Peardon, D. G. Richards, and C. E. Thomas (Hadron Spectrum Collaboration), Phys. Rev. D **83**, 071504 (2011).
[30] J. J. Dudek, R. G. Edwards, and C. E. Thomas (Hadron Spectrum Collaboration), Phys. Rev. D **86**, 034031 (2012).
[31] T. Yagi, S. Hashimoto, O. Morimatsu, and M. Ohtani, arXiv:1108.2970.
[32] Q. Liu, Proc. Sci., LAT (2009) 101 [arXiv:0910.2658].
[33] Z. Fu, Commun. Theor. Phys. **57**, 78 (2012).

[34] G. P. Lepage, in *Proceedings of TASI'89 Summer School*, edited by T. DeGrand and D. Toussaint (World Scientific, Singapore, 1990), p. 97.
[35] L. Maiani and M. Testa, Phys. Lett. B **245**, 585 (1990).
[36] M. Lüscher, Commun. Math. Phys. **105**, 153 (1986).
[37] M. Lüscher, Nucl. Phys. **B354**, 531 (1991).
[38] M. Luscher and U. Wolff, Nucl. Phys. **B339**, 222 (1990).
[39] K. Rummukainen and S. A. Gottlieb, Nucl. Phys. **B450**, 397 (1995).
[40] S. R. Beane, P. F. Bedaque, A. Parreño, and M. J. Savage, Phys. Lett. B **585**, 106 (2004).
[41] C. h. Kim, C. T. Sachrajda, and S. R. Sharpe, Nucl. Phys. **B727**, 218 (2005).
[42] N. H. Christ, C. Kim, and T. Yamazaki, Phys. Rev. D **72**, 114506 (2005).
[43] X. Feng, X. Li, and C. Liu, Phys. Rev. D **70**, 014505 (2004).
[44] C. B. Lang, D. Mohler, S. Prelovsek, and M. Vidmar, Phys. Rev. D **84**, 054503 (2011).
[45] Z. Fu, Phys. Rev. D **85**, 014506 (2012).
[46] L. Leskovec and S. Prelovsek, Phys. Rev. D **85**, 114507 (2012).
[47] M. Doring, U. G. Meissner, E. Oset, and A. Rusetsky, Eur. Phys. J. A **48**, 114 (2012).
[48] R. A. Briceno and Z. Davoudi, arXiv:1212.3398.
[49] P. Guo, J. Dudek, R. Edwards, and A. P. Szczepaniak, arXiv:1211.0929.
[50] C. W. Bernard, T. Burch, K. Orginos, D. Toussaint, T. A. DeGrand, C. E. Detar, S. Datta, S. Gottlieb, Urs M. Heller, and R. Sugar, Phys. Rev. D **64**, 054506 (2001).
[51] C. Aubin, C. Bernard, C. DeTar, J. Osborn, S. Gottlieb, E. B. Gregory, D. Toussaint, U. M. Heller, J. E. Hetrick, and R. Sugar, Phys. Rev. D **70**, 094505 (2004).
[52] K. Orginos and D. Toussaint, Phys. Rev. D **59**, 014501 (1998); K. Orginos, D. Toussaint, and R. L. Sugar, Phys. Rev. D **60**, 054503 (1999); T. Blum, C. DeTar, S. Gottlieb, K. Rummukainen, Urs M. Heller, J. E. Hetrick, D. Toussaint, R. L. Sugar, and M. Wingate, Phys. Rev. D **55**, R1133 (1997); J. F. Lagaë and D. K. Sinclair, Phys. Rev. D **59**, 014511 (1998); G. P. Lepage, Phys. Rev. D **59**, 074502 (1999); C. W. Bernard *et al.* (MILC Collaboration), Phys. Rev. D **61**, 111502(R) (2000).
[53] Z. Fu, Phys. Rev. D **85**, 074501 (2012).
[54] Z. Fu, J. High Energy Phys. 07 (2012) 142.
[55] C. B. Lang, L. Leskovec, D. Mohler, and S. Prelovsek, Phys. Rev. D **86**, 054508 (2012).
[56] T. Blum *et al.*, Phys. Rev. D **84**, 114503 (2011).
[57] Z. Fu, J. High Energy Phys. 01 (2012) 017.
[58] Z. Fu and K. Fu, Phys. Rev. D **86**, 094507 (2012).
[59] Z. Fu, Eur. Phys. J. C **72**, 2159 (2012).
[60] Z. Fu, arXiv:1210.5185.
[61] T. DeGrand and C. E. Detar, *Lattice Methods for Quantum Chromodynamics* (World Scientific, New Jersey, USA, 2006), p. 345.
[62] S. Dürr, C. Hoelbling, and U. Wenger, Phys. Rev. D **70**, 094502 (2004); C. Bernard, Phys. Rev. D **73**, 114503 (2006); C. Bernard, M. Golterman, Y. Shamir, and S. R. Sharpe, Phys. Lett. B **649**, 235 (2007); C. Bernard, M. Golterman, and Y. Shamir, Phys. Rev. D **73**, 114511 (2006); M. Creutz, Phys. Lett. B **649**, 241 (2007); S. Dürr and C. Hoelbling, Phys. Rev. D **74**, 014513 (2006); A. Hasenfratz and R. Hoffmann, Phys. Rev. D **74**, 014511 (2006).
[63] M. Albaladejo and J. A. Oller, Phys. Rev. Lett. **101**, 252002 (2008).
[64] C. Hanhart, Phys. Lett. B **715**, 170 (2012).
[65] M. Doring, U.-G. Meissner, E. Oset, and A. Rusetsky, Eur. Phys. J. A **47**, 139 (2011).
[66] D. Barkai, K. J. M. Moriarty, and C. Rebbi, Phys. Lett. **156B**, 385 (1985); A. Mihaly, H. R. Fiebig, H. Markum, and K. Rabitsch, Phys. Rev. D **55**, 3077 (1997); A. Mihály, Ph.D. thesis, Lajos Kossuth University, Debrecen, 1998.
[67] T. Umeda, Phys. Rev. D **75**, 094502 (2007).
[68] C. Aubin, C. Bernard, C. DeTar, J. Osborn, S. Gottlieb, E. B. Gregory, D. Toussaint, U. M. Heller, J. E. Hetrick, and R. Sugar (MILC Collaboration), Phys. Rev. D **70**, 114501 (2004).
[69] M. G. Alford, W. Dimm, G. P. Lepage, G. Hockney, and P. B. Mackenzie, Phys. Lett. B **361**, 87 (1995).
[70] A. Bazavov *et al.* (MILC Collaboration), Rev. Mod. Phys. **82**, 1349 (2010).
[71] D. B. Kaplan, Phys. Lett. B **288**, 342 (1992); Y. Shamir, Nucl. Phys. **B406**, 90 (1993); Phys. Rev. D **59**, 054506 (1999).
[72] A. Hasenfratz and F. Knechtli, Phys. Rev. D **64**, 034504 (2001); T. A. DeGrand, A. Hasenfratz, and T. G. Kovacs, Phys. Rev. D **67**, 054501 (2003); T. DeGrand, Phys. Rev. D **69**, 014504 (2004); S. Durr, C. Hoelbling, and U. Wenger, Phys. Rev. D **70**, 094502 (2004).
[73] D. B. Renner, W. Schroers, R. Edwards, G. T. Fleming, Ph. Hägler, J. W. Negele, K. Orginos, A. V. Pochinski, and D. Richards (LHP Collaboration), Nucl. Phys. B, Proc. Suppl. **140**, 255 (2005); R. G. Edwards, G. T. Fleming, P. Hagler, J. W. Negele, K. Orginos, A. V. Pochinsky, D. B. Renner, D. G. Richards, and W. Schroers (LHPC Collaboration), Proc. Sci., LAT (2006) 056.
[74] C. Bernard, T. Burch, K. Orginos, D. Toussaint, T. A. DeGrand, C. DeTar, S. Gottlieb, Urs M. Heller, J. E. Hetrick, and B. Sugar, Phys. Rev. D **62**, 034503 (2000).
[75] G. P. Lepage and P. B. Mackenzie, Phys. Rev. D **48**, 2250 (1993).
[76] C. Bernard *et al.* (MILC Collaboration), Proc. Sci., LAT (2007) 090.
[77] Z. W. Fu, Chin. Phys. Lett. **28**, 081202 (2011); Z. W. Fu and C. DeTar, Chinese Phys. C **35**, 896 (2011); C. Bernard, C. E. DeTar, Z. Fu, and S. Prelovsek, Phys. Rev. D **76**, 094504 (2007); Z. Fu, Report No. UMI-32-34073, 2006.
[78] J. Nagata, S. Muroya, and A. Nakamura, Phys. Rev. C **80**, 045203 (2009).
[79] S. Prelovsek, T. Draper, C. B. Lang, M. Limmer, K.-F. Liu, N. Mathur, and D. Mohler, Phys. Rev. D **82**, 094507 (2010).
[80] G. P. Lepage, B. Clark, C. T. H. Davies, K. Hornbostel, P. B. Mackenzie, C. Morningstar, and H. Trottier, Nucl. Phys. B, Proc. Suppl. **106**, 12 (2002); C. Morningstar, Nucl. Phys. B, Proc. Suppl. **109**, 185 (2002); M. Wingate, J. Shigemitsu, C. T. H. Davies, G. P. Lepage, and H. D. Trottier, Phys. Rev. D **67**, 054505 (2003).
[81] W. H. Press, S. A. Teukolsky, W. T. Vetterling, and B. P. Flannery, *Numerical Recipes in C: The Art of Scientific Computing* (Cambridge University Press, New York, 1992), 2nd ed.

[82] W. Huyer and A. Neumaier, ACM Trans. Math. Softw. **35**, 9 (2008); Matlab implementation: http://www.mat.univie.ac.at/~neum/software/snobfit/; Python: http://reflectometry.org/danse/docs/snobfit/.
[83] P. F. Bedaque, I. Sato, and A. Walker-Loud, Phys. Rev. D **73**, 074501 (2006).
[84] K. Sasaki, N. Ishizuka, T. Yamazaki, and M. Oka (PACS-CS Collaboration), Prog. Theor. Phys. Suppl. **186**, 187 (2010).
[85] J. Gasser and H. Leutwyler, Nucl. Phys. **B250**, 465 (1985).
[86] J. Beringer *et al.* (Particle Data Group Collaboration), Phys. Rev. D **86**, 010001 (2012).
[87] R. Garcia-Martin, J. R. Pelaez, and F. J. Yndurain, Phys. Rev. D **76**, 074034 (2007).
[88] I. Caprini, Phys. Rev. D **77**, 114019 (2008).
[89] G. Colangelo, S. Durr, A. Juttner, L. Lellouch, H. Leutwyler, V. Lubicz, S. Necco, C. T. Sachrajda *et al.*, Eur. Phys. J. C **71**, 1695 (2011).
[90] A. Bazavov *et al.* (MILC Collaboration), Proc. Sci., CD 09 (2009) 007 [arXiv:0910.2966].
[91] M. J. Savage, Prog. Part. Nucl. Phys. **67**, 140 (2012).
[92] J. A. Oller, E. Oset, and J. R. Pelaez, Phys. Rev. D **59**, 074001 (1999); F. Guerrero and J. A. Oller, Nucl. Phys. **B537**, 459 (1999).
[93] S. He, X. Feng, and C. Liu, J. High Energy Phys. 07 (2005) 011; M. Doring and U. G. Meissner, J. High Energy Phys. 01 (2012) 009; M. T. Hansen and S. R. Sharpe, Phys. Rev. D **86**, 016007 (2012); C. Liu, X. Feng, and S. He, Int. J. Mod. Phys. A **21**, 847 (2006); N. Li and C. Liu, Phys. Rev. D **87**, 014502 (2013).
[94] The numerical calculations of this work were unceasingly carried out for more than two years. We should especially thank Prof. Hou Qing's continuous encouragements and comprehensive support. Without his kind and selfless help, it would not have been possible for us to launch this work and have an opportunity to complete it.